Auckland
**Regional** Council
TE RAUHITANGA TAIAO

# Verification of Firth of Thames
# Hydrodynamic Model

May 2007   Technical Publication 326

*Printed on recycled paper*

# Verification of Firth of Thames hydrodynamic model

J. Oldman
J. Hong
S. Stephens
N. Broekhuizen

**Prepared for**

Auckland Regional Council

# Contents

Reviewed by:                                        Approved for release by:

*M C Hadfield*

Mark Hadfield                                       Rob Bell

Formatting checked

*A. Bartley*

# 1  Executive Summary

In 2003 the Auckland Regional Council contracted NIWA to undertake an ecological sustainability assessment for aquaculture in the Firth of Thames. The work was undertaken using a hydrodynamic model to simulate physical conditions in the Firth (Stephens 2003), and this was coupled with a biological model (Broekhuizen et al. 2004). To verify the hydrodynamic model it was re-run and compared with field data collected near Waimangu Point during April 2001 (Zeldis et al. 2001). This work complements another verification against data gathered at Wilson Bay in the eastern Firth (Broekhuizen et al. 2005).

Coastal currents arise from several contributing sources such as the tide, winds, oceanic currents, river plumes and water column stratification. Residual currents refer to all of the above factors except tides.

When comparing model and field data the spatial resolution of the model most be taken into account. For example, the Firth of Thames model has a horizontal resolution of 750 m and a vertical resolution of 2 m. Within each cell (measuring 750 by 750 m) and layers the model predicts the average value of any given parameter (e.g., salinity, current speed). Field data consist of measurements at a single point in space and at a fixed distance above the bed. Unless the model matches the horizontally and vertically spatial scale at which changes in field data occurs (as is the case for tide height) there will always be some degree of mismatch between model and field data.

<u>Tide heights</u>

This verification shows that the model predicts the tide heights very well. At least 98% of the variation in water level due to tides alone is accounted for by the model.

<u>Tidal currents</u>

This verification shows that the model simulates tidal currents well. At least 90% of variation of the dominant north-south tidal component is accounted for with the model. Tidal currents in the east-west direction are generally around one-tenth of the magnitude of the north-south component and the model accounts for 10–50% of the variation of the east-west component of the tidal current. Peak tidal currents are predicted to occur within 15 minutes of observed peak tidal currents and the direction of the peak flows are predicted to be within 2-10 ° of the observed peak tidal flows.

<u>Stratification</u>

The model predicts the depth-averaged temperature and salinity reasonably well but stratification is not well represented in the model in the vicinity of Waimangu Point. To improve the calibration it may be necessary to use a different vertical-mixing scheme in the model. Or alternatively it may simply be that the forcing data supplied to the model (e.g., wind, Outer Gulf intrusions, freshwater inflow) is insufficient.

<u>Residual (non-tidal) currents</u>

Several factors suggest that the model is not accurately re-producing the residual (non-tidal) currents at the Waimangu Point site:

- The model is unlikely to accurately re-produce vertically sheared flow in the absence of accurate stratification.

- At the southern site there is a reasonably good match between the current components near the sea-bed. The model generally over-predicts the north-south component. Near the surface the model under-predicts the magnitude of the east-west component of current.

- Cumulative drift is poorly re-produced at the northern comparison site with the model under-predicting the magnitude of the cumulative drift over the period of the verification.

The poor cumulative drift comparisons at the surface suggest that the input wind fields may not be accurate, but this could also result directly from lack of stratification in the model at this site.

Our opinion is that further effort on improving the accuracy of the hydrodynamic model of the Firth of Thames is not warranted unless a substantial and specifically-targeted field program is designed and implemented to provide the necessary database. The calibration (Stephens 2003), this verification and that of (Broekhuizen et al. 2005) have been undertaken using limited datasets, and the model provided a reasonable match given the data limitations. Caution must be exercised when interpreting this verification because of the very spatially localised area of comparison. There may be localised influences such as peculiarities in the bathymetry near current-meters, inaccurate specification of poorly documented river sources, and topographic influences on the wind at sites close to land that a large-scale model cannot perfectly reproduce, despite performing well over much of the domain.

The key outcome of this body of work is to determine the ecological sustainability of large-scale aquaculture in the Firth. The simulation models of plankton dynamics are driven by output from the hydrodynamic model.

We consider that the identified short comings of the present hydrodynamic model have a minor influence upon estimates of farm-scale plankton change.

In general the model under-predicts the residual currents at the Waimangu Point sites with the poorest calibration nearer the sea surface. It is unclear if this occurs in other areas of the Firth. We suggest that subtle changes in hydrodynamics, resulting from an improved calibration of the model (i.e., somewhat higher residual currents) may result in lower predictions of farm influences by the biological model at the local-scale. Improvement to the hydrodynamic model may also lead to the far-field extent of the farm footprint to be greater which will be offset by the changes in local-scale effects. In addition, when averaged over periods of weeks-to-months, the resultant time-averaged footprints are likely to be extremely insensitive to the magnitude of the discrepancy between observed and simulated residual currents.

We believe that consideration of the ensemble results from previous work still provide a useful guide as to the likely magnitude of local-scale and Firth-scale magnitudes of change due to the simulated farm layouts.  We acknowledge that there is a possibility that the precise geographic location of a particular isocline of change might be less well simulated, but we believe that the results still provide a useful guide in this respect, in lieu of embarking on an extensive field programme and undertaking modelling on a higher resolution grid.

The implications of deficiencies in the model verification were explored in a separate piece of work for Environment Waikato, in which the sensitivity of the plankton models to hydrodynamic forcing were investigated. Results from this sensitivity analysis are presented as Addendum 1 to this report.

# 2  Introduction and scope of work

In 2003 the Auckland Regional Council contracted NIWA to undertake an ecological sustainability assessment for aquaculture in the Firth of Thames. The work was undertaken using a hydrodynamic model to simulate physical conditions in the Firth (Stephens 2003), and this was coupled with a biological model (Broekhuizen et al. 2004). A two-year moratorium on the allocation of new aquaculture rights provided a tight timeframe for research and decision-making. Therefore, simulations were undertaken with only limited data available for calibration, on the basis that the simulations would still provide valuable baseline information to assist management questions. The hydrodynamic model was initially calibrated for temperature based on data from a single long-term mooring site in the central Firth (Figure 1), and for tides (levels and flows) based on harmonic analyses of historical current and water level measurements. No current-meter measurements were available to assess residual flows or to assist with calibration of momentum dispersion in the model.

At a meeting in Hamilton on 9 November 2004, the limitations of the hydrodynamic model calibration were discussed. As a result an extra data set collected near Waimangu Point (Figure 1) was subsequently made available by the Western Firth Consortium for verification of the hydrodynamic model. The Waimangu Point data set provides an opportunity to verify the model's performance in the eastern Firth of Thames.

For the present work the hydrodynamic model was re-run with the same parameter setup as in the original work (Stephens 2003) and compared with field data collected near Waimangu Point during April 2001 (Zeldis et al. 2001). This work complements another verification against data gathered at Wilson Bay in the eastern Firth (Broekhuizen et al. 2005).

This report presents a verification of the Firth of Thames hydrodynamic model. The hydrodynamic model was developed to predict physical conditions in the Firth, so that, when coupled with a biological model, predictions could be made about the extent of plankton depletion resulting from different scales of development of mussel farming. The verification described in this report revealed some deficiencies in the hydrodynamic model. The implications of this were explored in a separate piece of work for Environment Waikato, in which the sensitivity of the plankton models to hydrodynamic forcing were investigated. Although Environment Waikato requested the additional work, its content draws heavily upon work that has been funded by New Zealand's Foundation for Research and Science and Technology through NIWA's Sustainable Aquaculture Program (contract CO1X0507). Results from this sensitivity analysis are presented as Addendum 1 to this report.

**Figure 1.**
Firth of Thames 750 m bathymetry grid; colour-scale indicates depth (m). ADP current-meter sites are marked '⊗', nearby CTD cast sites shown in Figure 9 and Figure 10 are marked •, river sources are

marked 'x', and the FoT mooring site is marked '+'. The *I* and *J* indices on the two axes indicate the grid-cell coordinates (each grid cell is 750 m x 750 m horizontally).
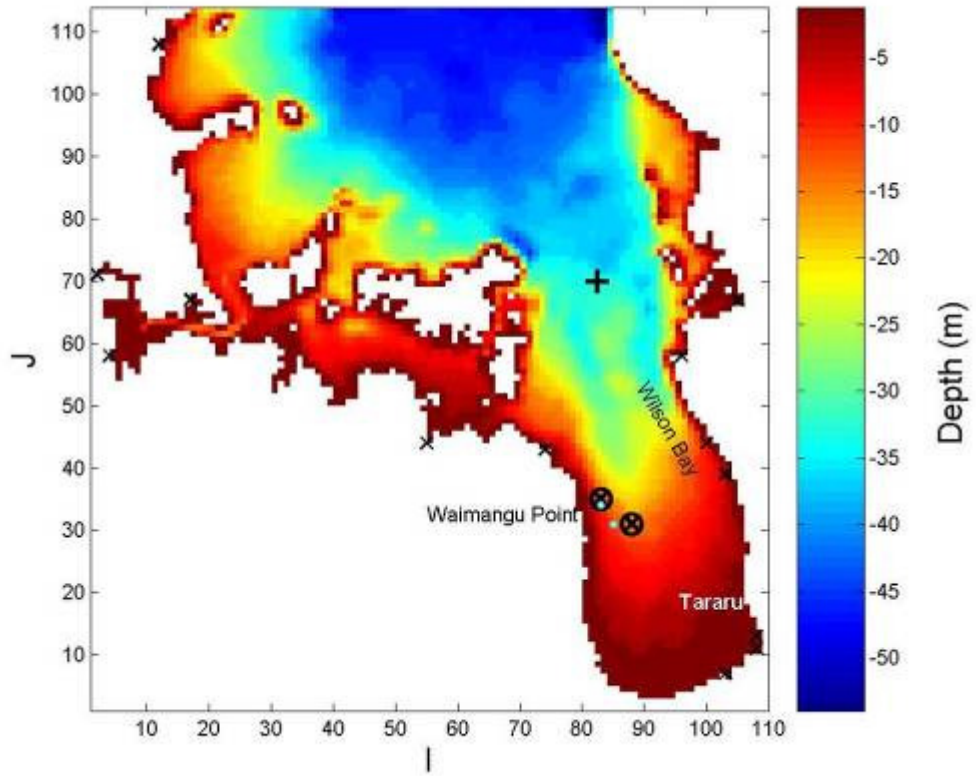
# 3 Modelling methods

The present report describes a verification simulation of the calibrated three dimensional hydrodynamic model described by Stephens (2003). The purpose of a verification simulation is to test the performance of a previously calibrated model against data other than those used to calibrate it. Thus the internal model parameters remain unchanged between the verification and calibration simulations. In the present case the time period of the verification simulation differs from that of the calibration simulation, so only the data used to force the model (e.g., tidal water levels at the open northern boundary, air temperature, wind stress, river flows) are changed.

The reader is referred to Stephens 2003 for a description of the model set-up, e.g., bathymetry, vertical grid structure, seabed resistance, turbulence closure scheme, heat-exchange coefficients, and specification of input data. Importantly, the model has a horizontal resolution of 750 m and a vertical layering setup giving a variable top layer (of up to 6.5 m) and subsequent layers of 2 m

The time period of the verification simulation was 1–29 April 2001, bracketing the deployment of two ADP (Acoustic Doppler Profiler) current-meters from 4–20 April 2001 and two synoptic CTD (Conductivity, Temperature, Depth) surveys on 5th and 20th April 2001 near Waimangu Point (Figure 1).

Whilst it is conceivable that large-scale farm development may modify flow patterns, this has not been accounted for in our simulations. Initial studies have shown that currents do slow as they pass through marine farms, but the extent of retardation is not well known. Enhanced friction and slower flows will affect the amount of time that material is held inside the farm domain, and will therefore affect production estimates inside the farm area. The presence of farms is unlikely to modify the overall hydrodynamics in the Firth of Thames, and therefore should have only minor effect on transport well beyond the farms.

## 3.1 Forcing inputs to the model

Data used to force the model during the specified verification period are described here briefly.

### 3.1.1 Tide

The model was forced with tidal water level variations at the open-sea boundary of the model grid (along the north side of Figure 1). The tidal variation (Figure 2) was reconstructed from the 13 dominant tidal constituents; the phase and amplitude of each constituent was extracted from a larger EEZ model (Walters et al. 2001). The verification period spans both spring and neap tides.

**Figure 2.**

Sea-surface water level (metres above tide gauge zero) at Moturiki prescribed at the model's seaward boundary for April 2001. LINZ Moturiki Vertical Datum -1953 is 1.487 m above tide gauge zero.
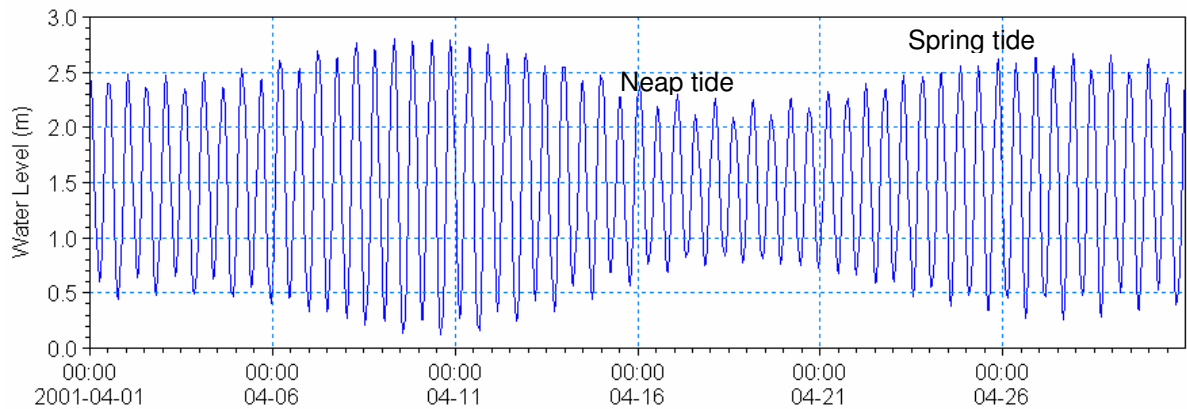


## 3.1.2  Water temperature

Aside from solar radiation inputs at the water surface, the model requires an initial temperature field over the whole model grid at a resolution of 750 m. It also requires water temperatures to be input at the open sea boundary (northern end) for the length of the verification period. Obtaining accurate initial temperature fields over the whole model is a challenging task because of naturally high spatial variability created by subtleties such as cloud cover and wind sheltering by islands. Furthermore, it is practically impossible to measure temperature everywhere on the open boundary to use as input, and initial conditions are often estimated for the same reasons.

## 3.1.3  Initial temperatures

Data from 3 sources were used to define the initial conditions for the verification simulation: 1. A near-bottom current-meter located in the central Firth (Figure 1); 2. A temperature mooring in the outer Hauraki Gulf (beyond the outer boundary of the model grid in Figure 1); 3. Sea surface temperature derived from satellite imagery of the Hauraki Gulf.

The temperature data from the outer Gulf mooring (measured 147.0 m above the bed in 162.0 m of water or 15 m below the surface) were used to define the initial temperature of the surface layer of the model on the open boundary (Figure 3). No temperature data down the water column were available for April 2001, so the temperature data from central Firth mooring (measured 9.0 m above the bed in 38.0 m of water) were applied as an initial temperature for the near-bed layer of the model on the open sea boundary. The temperatures in intermediate depth layers in the model were then linearly interpolated.

The spatial variation in initial sea-surface temperature across the Gulf was derived from the satellite imagery data. The same initial vertical temperature gradient (°C change per meter depth) that was applied at the open boundary was applied across the whole of the Gulf in lieu of no temperature-depth measurements elsewhere in the Firth.

### 3.1.4 Open-sea boundary water temperatures

The temperature data from the outer Gulf mooring (measured 15.0 m from the surface) were used to define the temperature of the surface layer of the model (which varies in thickness from 3.5-6.5 m) on the open-sea boundary (Figure 3) over the verification period. Similarly the temperature data from central Firth mooring (measured 9.0 m above the bed in 38.0 m of water) were applied to the near-bed layer of the model on the open-sea boundary over the verification period. Intermediate layers were then linearly interpolated.

Because the model was being run during April we specified a typical autumn river temperature of 16°C.

**Figure 3.**

Observed mean daily temperatures from the Outer Gulf mooring (147.0 m above the bed in 162.0 m of water) the Firth of Thames mooring (9.0 m above the bed in 38.0 m of water) for April 2001.
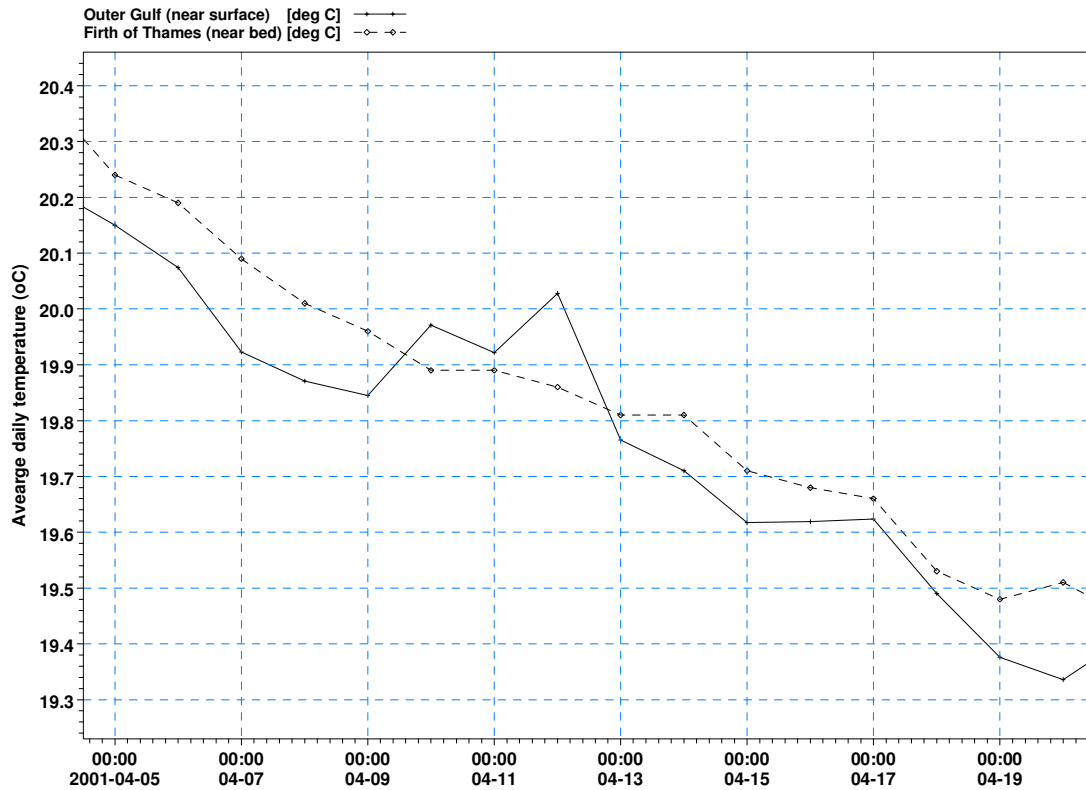


### 3.1.5  Salinity

As before, the open-sea boundary salinity was set to 35.5 psu (typical of ocean water) and the river salinities were set to 4 psu. The same initial salinity conditions were applied spatially across the Gulf and down the water column as used in Stephens (2003), as this pattern is reasonably representative for this time of year.

### 3.1.6  Wind and air pressure

Hourly wind data for the verification simulations were obtained from the same automated weather stations (AWS) as the previous study (Stephens 2003), except that no data for April 2001 were available from Whangaparoa. The remaining six stations are: Auckland Aero, Whangarei Aero, Mokohinau (Figure 4), Onehunga, Leigh2 and Paeroa.

Air pressure was included as part of meteorological forcing, using pressure data available from the following four weather stations: Auckland Aero, Whangarei Aero, Mokohinau and Paeroa.

These data were processed in the same way as before (Stephens 2003), duplicates were removed and gaps were filled using linear interpolation with the maximum allowed gap size of 6 hours, then the data from the six (four for pressure) stations were interpolated over the region using a cubed inverse-distance routine to provide a spatially-varying wind (or pressure) field.

The wind friction coefficient was set to its default value of 0.0026.

**Figure 4.**
Wind data used in numerical simulations (data from Mokohinau AWS is shown below). Data is plotted in meteorological convention (feathers project in the directions from which the wind blows).
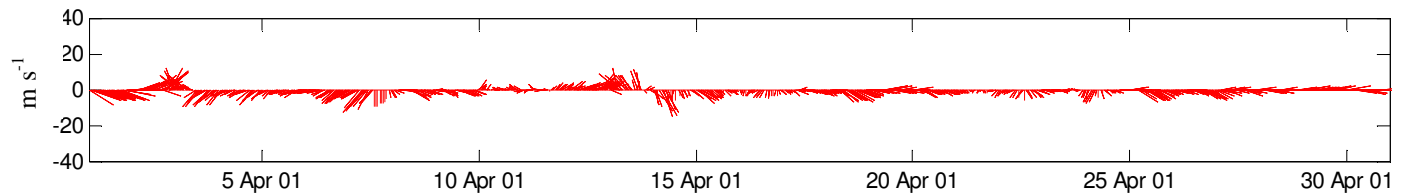


### 3.1.7 Rivers

During the calibration simulations (Stephens 2003), river source flows were specified in the model at 13 sites for the month of March using long-term average flows, combining data from automatic flow gauging sites supplemented by estimated runoff (Hadfield et al. 2002). For the verification, the three major rivers (Piako, Waihou and Kauaeranga) located on the southern Firth, daily discharge data were input to the model. These three sources supply most of the freshwater to the Firth. Note that no river source was included in the model from the Waimangu Stream near Waimangu Point (Figure 1), as there was no readily-available flow information for this stream and its omission was considered to be of minor importance to the overall hydrodynamics of the Firth during the initial simulations (Stephens 2003). However, the Waimangu Stream would cause localised effects on stratification and possibly currents, and the neglect of these may impact upon the verification against data collected at the nearby northern ADP site (Figure 1). The ten minor sources were adjusted to appropriate flows for April 2001, by applying a scaling factor of 2.1. The scaling factor was obtained from comparison of average flow during April 2001 with average monthly flows in March used by Stephens (2003).

### 3.1.8 Air temperature and relative humidity

Dry-bulb temperature readings from Auckland Aero, Whangarei Aero, Mokohinau, Onehunga, Leigh2 and Paeroa weather stations were averaged to create an hourly temperature timeseries for input to the model (Figure 5).

Humidity is an important control on air-sea heat exchange which in turn affects sea temperature. In the absence of sea-based measurements, relative humidity measurements from land-based weather stations were trialled in the previous study, but these were not proven to provide any better results than the default value of 88%, so relative humidity was set to 88% again for the verification.

**Figure 5.**
Air temperature time series used for model simulations.
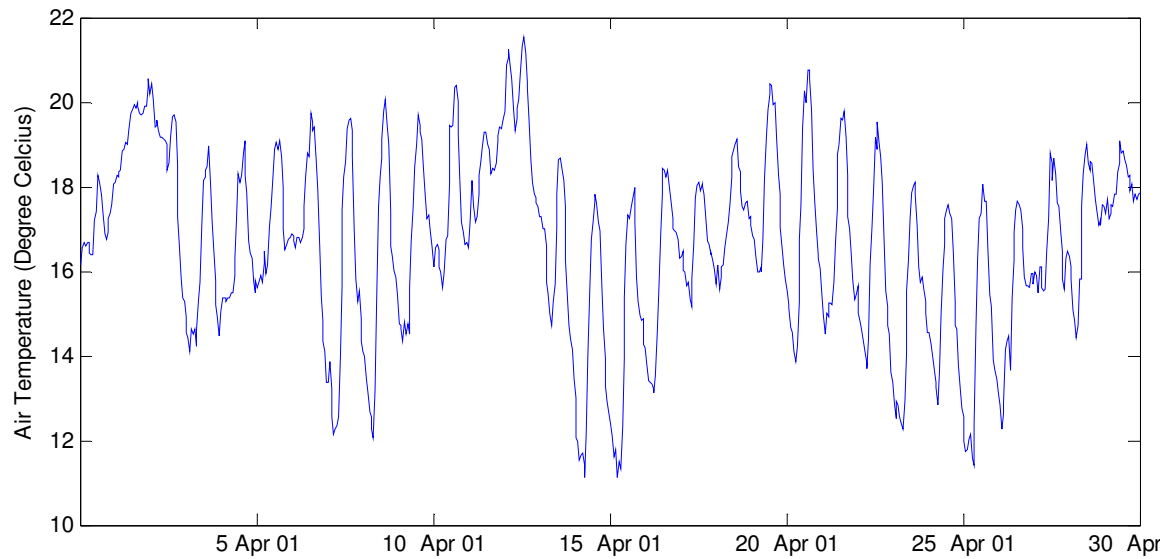


## 3.2 Model output

Water flow velocity in the horizontal and vertical directions, water level, temperature and salinity were output at ½-hour intervals.

# 4 Model verification

## 4.1 Tides

The simulation for April 2001 resulted in a good agreement between the relevant model cell and tide-height measurements from the Tararu tide gauge on the southern Firth of Thames (Figure 1) in terms of both tidal range and phase (Figure 6 and Figure 7). Figure 8 shows the water level verification against data from northern ADP near Waimangu Point. The r-squared value (0.98) slope (0.995) and offset (0.0004) show that the model provides excellent predictions of water levels at Waimangu Point. Overall the model is a good predictor of water levels across the Firth of Thames.

**Figure 6.**
Water levels from verification model simulation and measurement from Tararu tide gauge.
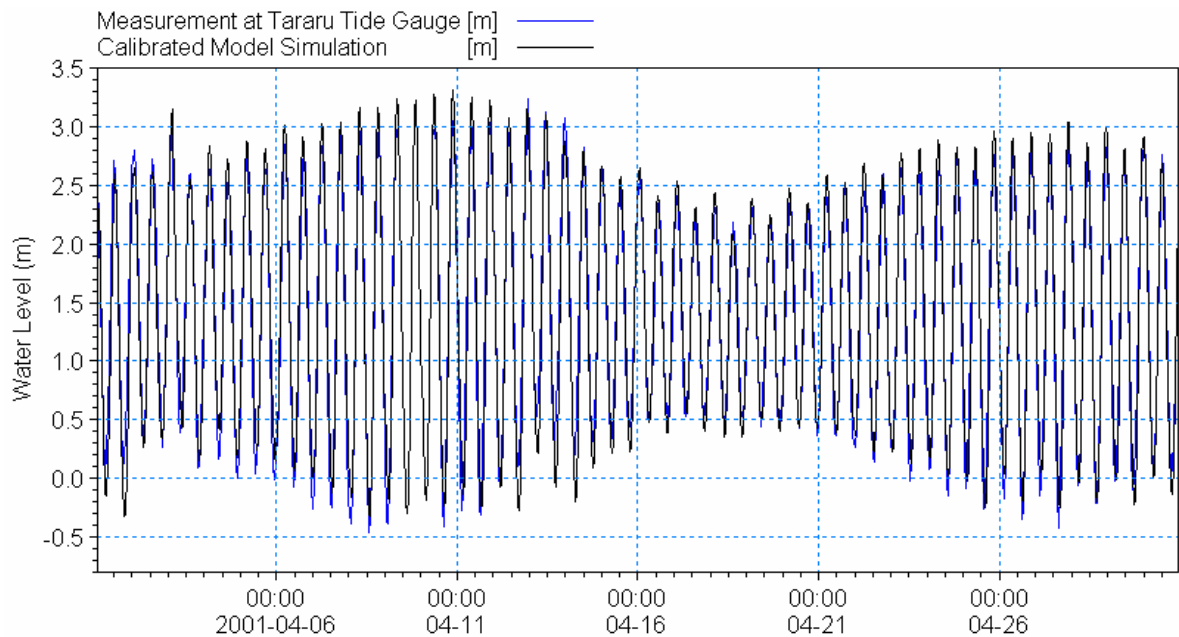
**Figure 7.**

Regression plot of water levels for verification model simulation against measurement at Tararu tide gauge.
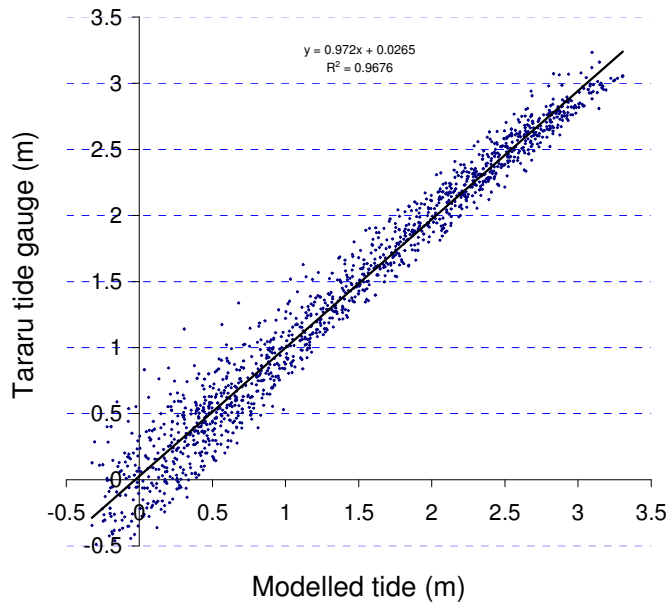


**Figure 8.**

Regression plot of water levels for verification model simulation against measurement at northern ADP site.
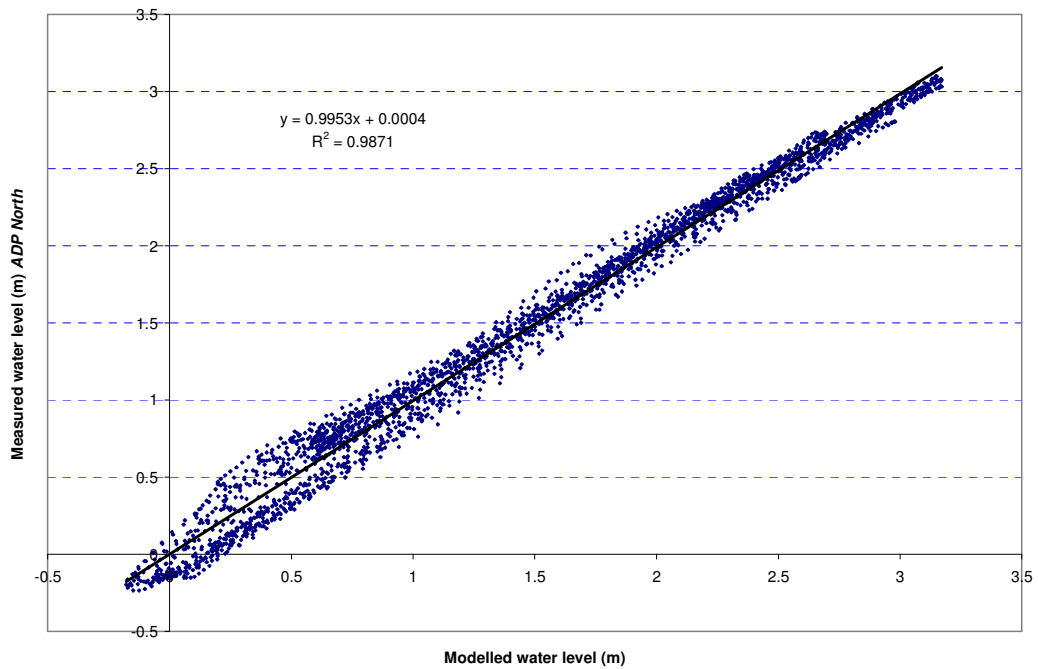
## 4.2　Stratification

Figures 9–10 compare measured and modelled salinity and temperature respectively, on 20th April 2001 when CTD measurements were available. The preceding week had been dry with moderate south-easterly winds. Although the general depth-averaged temperature and salinity match well, the plots show that the model is not reproducing the stratification with depth due to either temperature or salinity that is evident in the field data. Comparisons at other sites and during the first survey on 5th April are not shown but lead to similar conclusions.

Three sources of uncertainty could explain this mis-match:

1. The vertical dispersion of temperature and salinity is too high in the model resulting in less vertical stratification in the Waimangu Point vicinity.

2. The absence of Waimangu Stream inflow (which would lower both salinity and temperature locally) in the model reduces the ability of the model to reproduce the local stratification at the Waimangu site.

3. The assumptions made to estimate (in lieu of data) an initial salinity/temperature field and set the time-varying salinity/temperature condition on the open-sea boundary for all the model layers may be incorrect.

Further ramifications are discussed in the conclusions.

**Figure 9.**

Salinity (measured and modelled) on 20 April 2001 at sites marked '.' (near '⊗') in Figure 1: solid line = measured at northern site; dashed line = measured at southern site; triangles = simulated at northern site; diamonds = simulated at southern site.
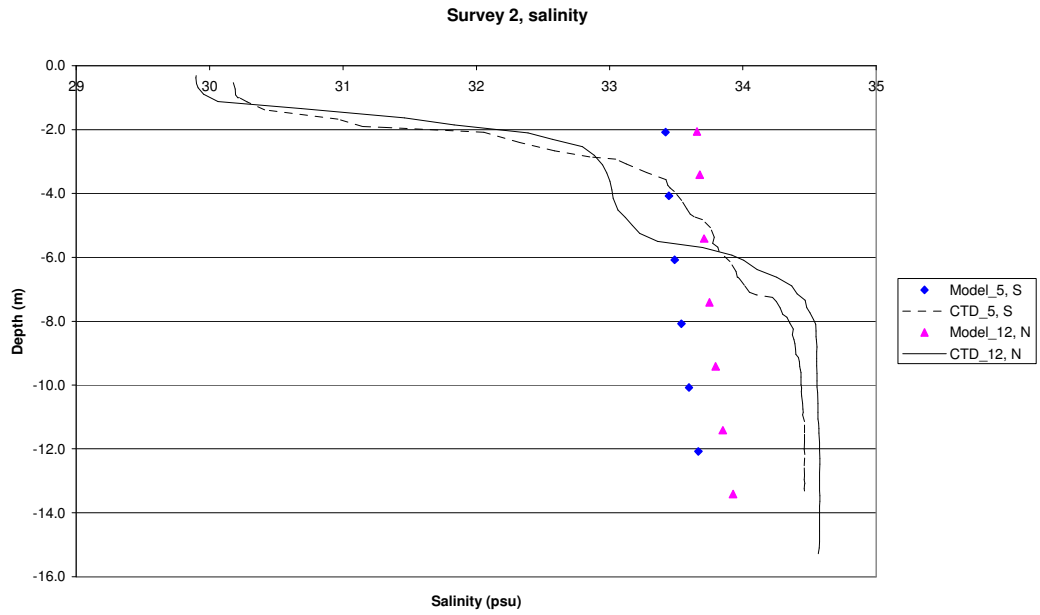
**Figure 10.**

Temperature (measured and modelled) on 20 April 2001 at sites marked ".' (near '⊗') in Figure 1: solid line = measured at northern site; dashed line = measured at southern site; triangles = simulated at northern site; diamonds = simulated at southern site.

**Survey 2, temperature**
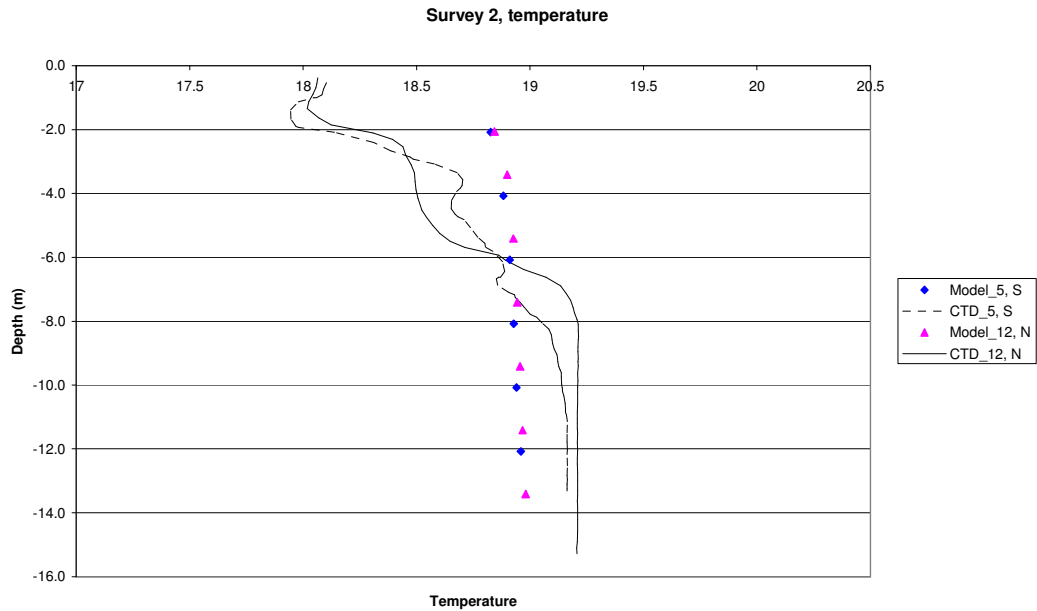


## 4.3    Currents

### Field data

Data from the field report (Zeldis et al. 2001) indicates that at the northern ADP site (Figure 1) currents predominantly flowed in an east-west orientation (Figure 11) whilst at the southern site the predominant current direction is north-south (i.e., longshore) (Figure 12). To explain this anomaly, we believe that the data (as presented by Zeldis et al. 2001) from the northern ADP site were transposed between cross-shore and alongshore components.

Comparison of the moored ADP data and the vessel-mounted current-profiles collected during the survey of the 4th of April 2001 shows that the moored data at the southern site is in good agreement with the data collected during the underway survey of the flooding tide of the 4th of April (Figure 13). However the uncorrected moored data from the north site shows strong offshore currents.

Subsequent analysis for the northern site assumes the measured north/south component is actually the negative east/west component and the measured east/west component is actually the negative north/south component.

**Figure 11.**

Figure 5.1.1.1 from NIWA Client Report: CHC01/44: Numbers of observations of direction of the current at various heights above the seabed from 4–20 Apr. 2001 at the *northern* site.
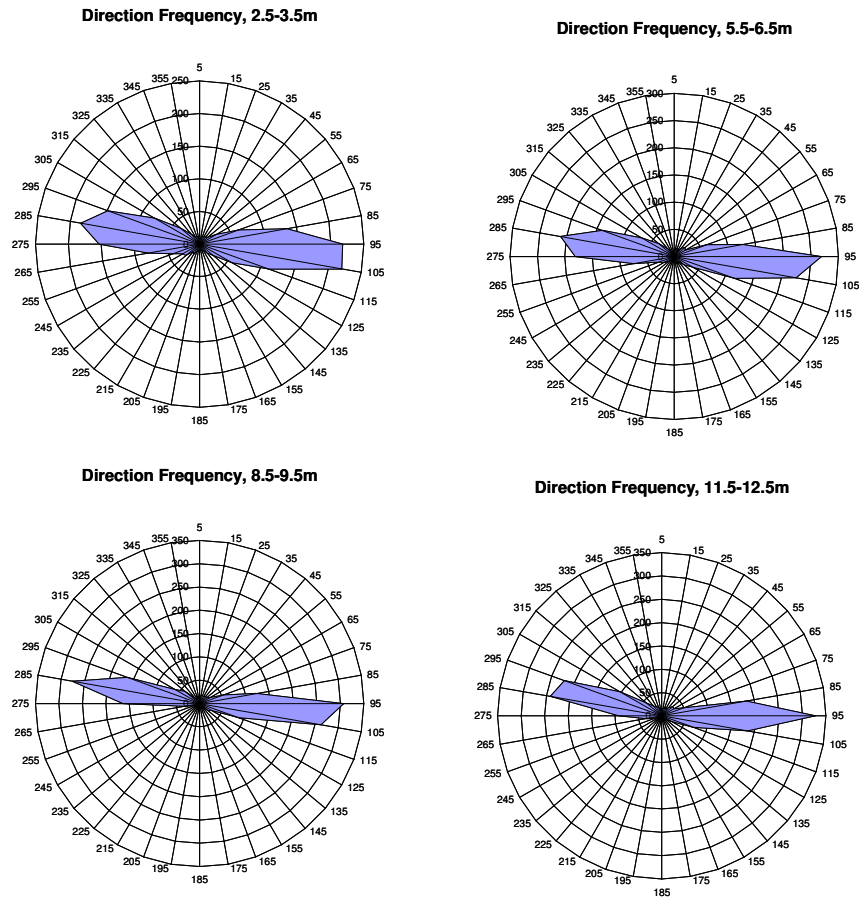
**Figure 12.**

Figure 5.1.2.1 from NIWA Client Report: CHC01/44: Numbers of observations of direction of the current at various heights above the seabed from 4–20 Apr. 2001 at the *southern* site.

**Direction Frequency, 2.5-3.5m**

**Direction Frequency, 5.5-6.5m**

**Direction Frequency, 8.5-9.5m**

**Direction Frequency, 11.5-12.5m**

**Direction Frequency, 14.5-15.5m**
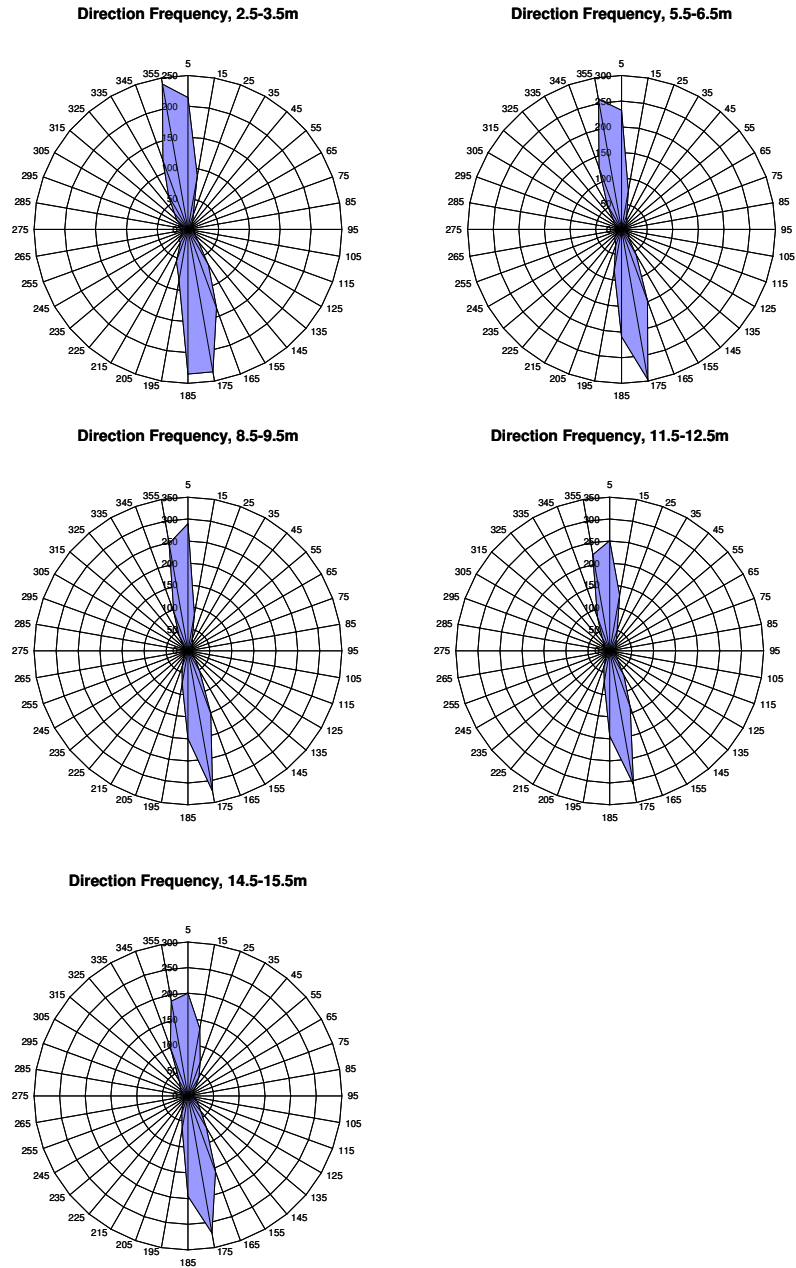
**Figure 13.**

Comparison of moored ADP data with ADP measurements from an underway survey during peak flooding tide on 4 April 2001.
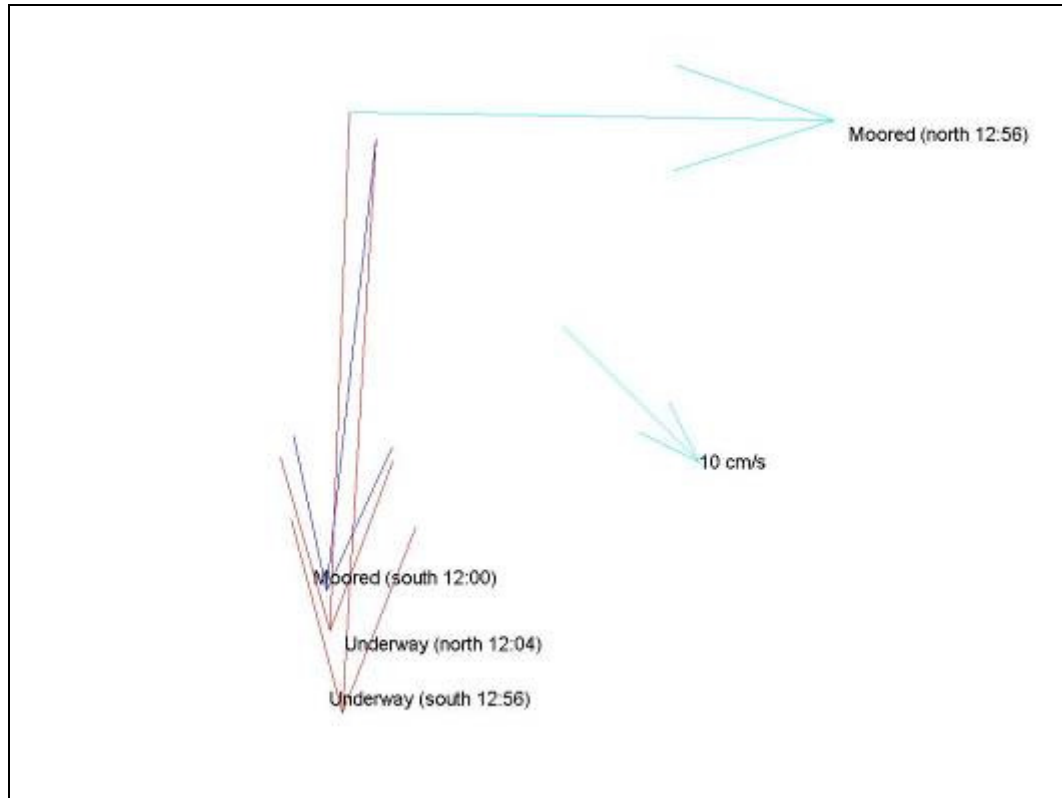


### 4.3.1  Current comparison

The field data from the ADP's were run through a low-pass filter to remove the high frequency signal observed in the data. This high frequency seiching (with a period of around 35 minutes) could not be resolved by the model driven by 3-hourly winds and longer period tides. Figure 14 shows scatter plots between simulated and measured depth-averaged currents at the ADP sites. The model generally predicted the predominant north-south component of the currents well (Figure 14a, c), but was less successful at predicting the smaller east-west component of the flow (Figure 14b, d).

**Figure 14.**

Scatter plot between simulated and measured depth-averaged current speeds in (A) north-south direction at the northern site, (B) east-west direction at the northern site, (C) north-south direction at the southern site, (D) east-west direction at the southern site.
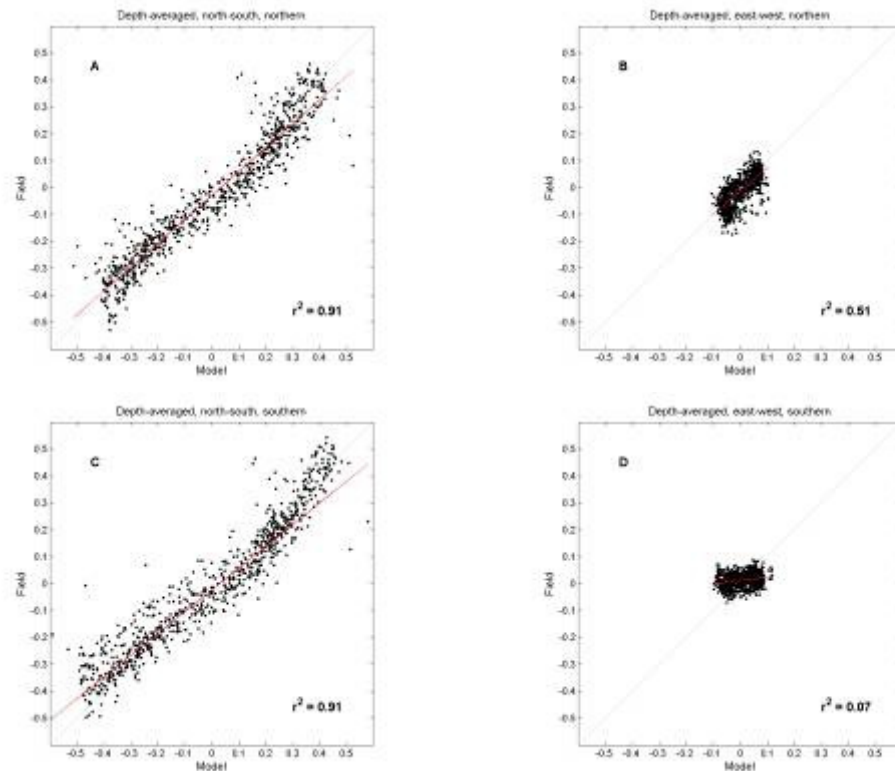


Table 1 gives statistics from linear regressions between the measured and simulated currents at the two sites, for both the north-south and east-west current components. The $r^2$ values show that the model explains >90% of the variance for currents flowing in the north-south direction, at both sites. The smaller east-west component of the current flow is poorly reproduced. This can be explained as follows. The tide dominates current flows in the Firth, and most of the tidal flow at these sites is in the north-south direction (as seen from the tidal inclinations in Table 2 & 3). The stronger correlations in the north-south direction reflect the dominance of tidal flows along this axis, and the reasonable simulation of tidal flows by the model (Figures 19–31 Appendix 1). The timeseries plots in Figures 32–44 (Appendix 1) show that the underlying pattern of flow in the east-west direction is tidal in the model, but in the measured currents the underlying tidal contribution is substantially complicated by other signals. The east-west current component is relatively weakly influenced by the tide, and other forcings such as wind and buoyancy are relatively more important. Although these mechanisms are smaller compared with the tidal effect, their cumulative effect is important in terms of the east-west component of residual drift that can advect larvae in the water column. The model does not appear to be reproducing

these minor (residual) processes well, in this location. The poor correlation between the east-west current components may result from either or a combination of: 1. Inadequate spatial resolution of the wind field over sea in the Firth, due to lack of localised wind measurements; 2. Absence of localised stratification effects from the Waimangu Stream and associated buoyancy forcing that would also contribute to incorrect representation of momentum transfer from wind stress; 3. Inadequate calibration of the relevant momentum transfer equations leading to poor representation of momentum transfer from wind stress. These issues are discussed further in the conclusions.

Table 2 and Table 3 compare $M_2$ tidal current characteristics (i.e., mean tide range[1]) from harmonic analysis of measured and simulated currents at the northern and southern sites respectively. Tidal current characteristics are summarised in the form of an ellipse defined by a major (long) axis and minor (short) axis, a phase when the peak north-going current occurs (relative to New Zealand Standard Time) and an inclination of major axis (relative to True East).Results indicate that simulated $M_2$ tidal current speeds are faster than those measured by up to 22% (median 11%), with the discrepancy becoming greater further from the seabed. The linear regression slopes in Table 1 also show that the model increasingly over-predicts current speeds near the water surface. As outlined in the verification process at Wilson Bay (Broekhuizen et al. 2005) this may be corrected by altering the models vertical mixing (through the Smagorinsky formulation). The maximum difference in the phasing (8.2 °) equates to a maximum 17 minute difference in the timing of the peak tidal flows (with the actual peak tidal flow occurring slightly earlier than predicted). The inclination data shows that the direction of the peak tidal flow at the northern site is predicted to within 2.5 ° of the measured peak tidal flow direction. At the southern site the model consistently predicts that peak tidal currents will run slightly anti-clockwise of the measured data (i.e., inclinations are all negative and in the range 3.1–12.6 °).

---

[1] Only the $M_2$ tidal component can be adequately resolved from the 16-day ADP record.

**Table 1a.**

Linear regression statistics for currents at the northern site. ADP (measured) = Slope × Model (simulated) + Offset.

| Northern site | Height above seabed (m) | Slope | Offset | $r^2$ |
|---|---|---|---|---|
| North-south component | 12 | 0.7829 | - 0.0101 | 0.8691 |
| | 10 | 0.7990 | + 0.0043 | 0.8814 |
| | 8 | 0.8184 | - 0.0005 | 0.8878 |
| | 6 | 0.8371 | + 0.0045 | 0.8809 |
| | 4 | 0.8563 | + 0.0031 | 0.8815 |
| | 2 | 0.8384 | + 0.0035 | 0.8596 |
| East-west component | 12 | 0.6301 | + 0.0039 | 0.3019 |
| | 10 | 0.7590 | + 0.0022 | 0.4878 |
| | 8 | 0.7391 | - 0.0003 | 0.4684 |
| | 6 | 0.6457 | - 0.0022 | 0.3313 |
| | 4 | 0.4846 | - 0.0022 | 0.1794 |
| | 2 | 0.3548 | - 0.0118 | 0.0956 |

**Table 1b.**

Linear regression statistics for currents at the southern site. ADP (measured) = Slope × Model (simulated) + Offset.

| North-south component | 14 | 0.7258 | + 0.0008 | 0.8793 |
|---|---|---|---|---|
| | 12 | 0.7741 | + 0.0072 | 0.8945 |
| | 10 | 0.8124 | + 0.0111 | 0.8991 |
| | 8 | 0.8479 | + 0.0130 | 0.8987 |
| | 6 | 0.8880 | + 0.0150 | 0.8929 |
| | 4 | 0.9204 | + 0.0171 | 0.8892 |
| | 2 | 0.9662 | + 0.0173 | 0.8690 |

| East-west component | 14 | 0.1838 | + 0.0045 | 0.0447 |
| | 12 | 0.0830 | + 0.0002 | 0.0183 |
| | 10 | 0.1148 | - 0.0005 | 0.0399 |
| | 8 | 0.2148 | - 0.0020 | 0.1215 |
| | 6 | 0.3036 | - 0.0036 | 0.1807 |
| | 4 | 0.3902 | - 0.0045 | 0.2225 |
| | 2 | 0.5311 | + 0.0041 | 0.2103 |

**Table 2.**

$M_2$ tidal constituents from harmonic analysis of measured and simulated currents at the *northern* ADP site. Inclinations are specified in compass coordinates (clockwise relative to true north).

| Height above bed (m) | Field data | | | | Model data | | | | Difference | | | |
|---|---|---|---|---|---|---|---|---|---|---|---|---|
| | Major (m/s) | Minor (m/s) | Inclination ($^o$ from True East) | Phase (relative to NZST) | Major (m/s) | Minor (m/s) | Inclination | Phase | Major (m/s) | Minor (m/s) | Inclination ($^o$ from True East) | Phase (relative to NZST) |
| 2 | 0.260 | 0.048 | 101.4 | 293.3 | 0.289 | 0.020 | 103.1 | 287.7 | -0.029 | 0.028 | -1.7 | 5.6 |
| 4 | 0.298 | 0.048 | 102.0 | 296.4 | 0.324 | 0.013 | 102.5 | 291 | -0.026 | 0.035 | -0.5 | 5.4 |
| 6 | 0.321 | 0.037 | 101.5 | 299 | 0.352 | 0.004 | 101.8 | 294.1 | -0.031 | 0.033 | -0.3 | 4.9 |
| 8 | 0.331 | 0.022 | 103.0 | 302.4 | 0.376 | 0.005 | 101.2 | 296.6 | -0.045 | 0.017 | 1.8 | 5.8 |
| 10 | 0.345 | 0.005 | 103.2 | 305.1 | 0.394 | 0.011 | 100.8 | 298.2 | -0.049 | -0.006 | 2.4 | 6.9 |
| 12 | 0.352 | 0.002 | 103.0 | 307.3 | 0.410 | 0.014 | 100.8 | 299.1 | -0.058 | -0.012 | 2.2 | 8.2 |
| | | | | | | | | Min diff. | -0.058 | -0.012 | -1.7 | 4.9 |
| | | | | | | | | Max dif. | -0.026 | 0.035 | 2.4 | 8.2 |

**Table 3.**

$M_2$ tidal constituents from harmonic analysis of measured and simulated currents at the *southern* ADP site. Inclinations are specified in compass coordinates (clockwise relative to true north).

| Height above bed (m) | Field data | | | | Model data | | | | Difference | | | |
|---|---|---|---|---|---|---|---|---|---|---|---|---|
| | Major (m/s) | Minor (m/s) | Inclination (° from True East) | Phase (relative to NZST) | Major (m/s) | Minor (m/s) | Inclination | Phase | Major (m/s) | Minor (m/s) | Inclination (° from True East) | Phase (relative to NZST) |
| 2 | 0.279 | 0.024 | 93.9 | 292.6 | 0.260 | 0.020 | 97.0 | 290.5 | 0.019 | 0.004 | -3.1 | 2.1 |
| 4 | 0.308 | 0.012 | 93.8 | 295 | 0.311 | 0.023 | 100.0 | 292.2 | -0.003 | -0.011 | -6.2 | 2.8 |
| 6 | 0.326 | 0.004 | 93.3 | 298.6 | 0.348 | 0.017 | 101.0 | 294.8 | -0.022 | -0.013 | -7.7 | 3.8 |
| 8 | 0.343 | 0.012 | 92.7 | 301.7 | 0.379 | 0.004 | 101.6 | 297.7 | -0.036 | 0.008 | -8.9 | 4.0 |
| 10 | 0.348 | 0.022 | 91.3 | 303.9 | 0.407 | 0.011 | 101.8 | 300.4 | -0.059 | 0.011 | -10.5 | 3.5 |
| 12 | 0.349 | 0.031 | 89.2 | 305.4 | 0.427 | 0.023 | 101.8 | 302.4 | -0.078 | 0.008 | -12.6 | 3.0 |
| | | | | | | | | Min diff. | -0.078 | -0.011 | -12.6 | 2.1 |
| | | | | | | | | Max dif. | 0.019 | 0.013 | -3.1 | 4.0 |

## Cumulative drift comparison

Cumulative drift plots of the filtered currents at both ADP deployments sites are shown in Figure 15–18, for near-bed and near-surface examples (cumulative vector plots at other depths are included in Appendix 2, Figures 45–53).

At the southern ADP site the model appears to predict the current drift well, with the exception of the surface layer. Again, the agreement between model and data is best near the seabed (Figure 15), decreasing toward the surface, but the drift patterns are in general agreement throughout much of the water column. This suggests the model is reproducing residual current flow well except close to the water surface, where local wind variability is unlikely to be well represented in the model. An additional factor to consider is the layering used within the model. The layer thickness defined by Stephens (2003) was defined as 2 m. However this layer thickness only applies to sub-surface layers. The thickness of the surface layer varies between 2.0 m (at low water) through to 4.8 m (at high water) and the model outputs the average value throughout this layer. Thus, when the surface layer is shallower the effect of wind shear will be more significant than at high water.

At the northern ADP site the agreement between the model and data is poor; there is a southward drift evident in the field data that is not reproduced by the model (e.g., Figure 18). We are unsure as to the cause of the discrepancy at the northern site, but it could be influenced by localised wind patterns not available for model input, and/or by incorrect representation of stratification due to the absence of the Waimangu Stream source.

**Figure 15.**

Cumulative vector plot of current drift 2 m above the seabed at the southern ADP site. Both measured and modelled drift paths start at 0, 0. Red = measured by ADP, blue = simulated by model. Numbers 1–16 mark days since ADP deployment.  North arrow indicates True North. North arrow indicates True North.
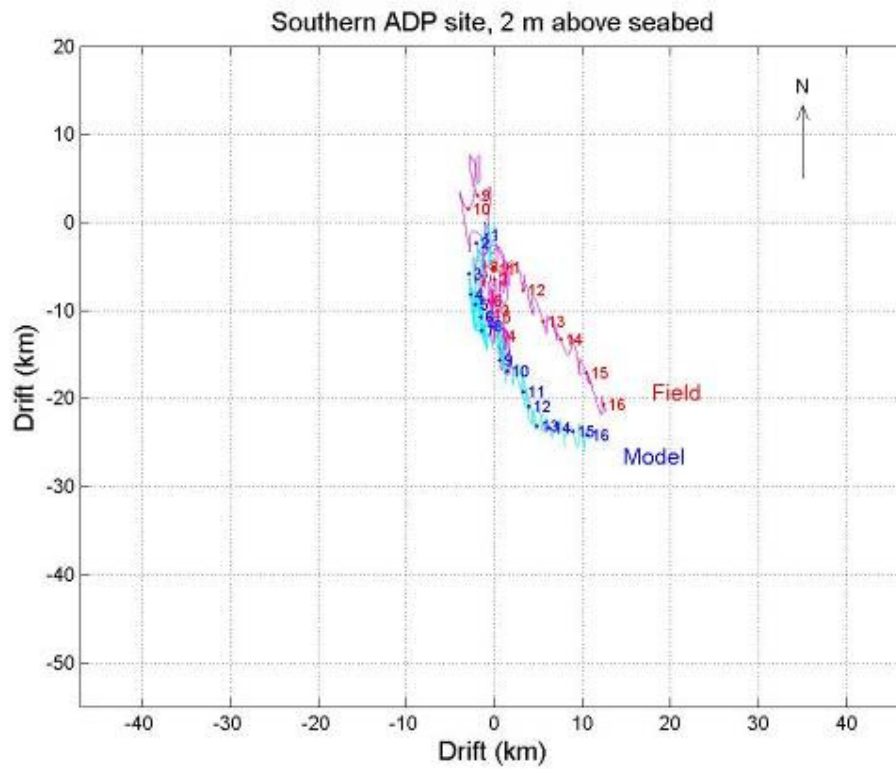
**Figure 16.**

Cumulative vector plot of current drift 14 m above the seabed (near surface) at the southern ADP site. Both measured and modelled drift paths start at 0, 0. Red = measured by ADP, blue = simulated by model. Numbers 1–16 mark days since ADP deployment. North arrow indicates True North. North arrow indicates True North.
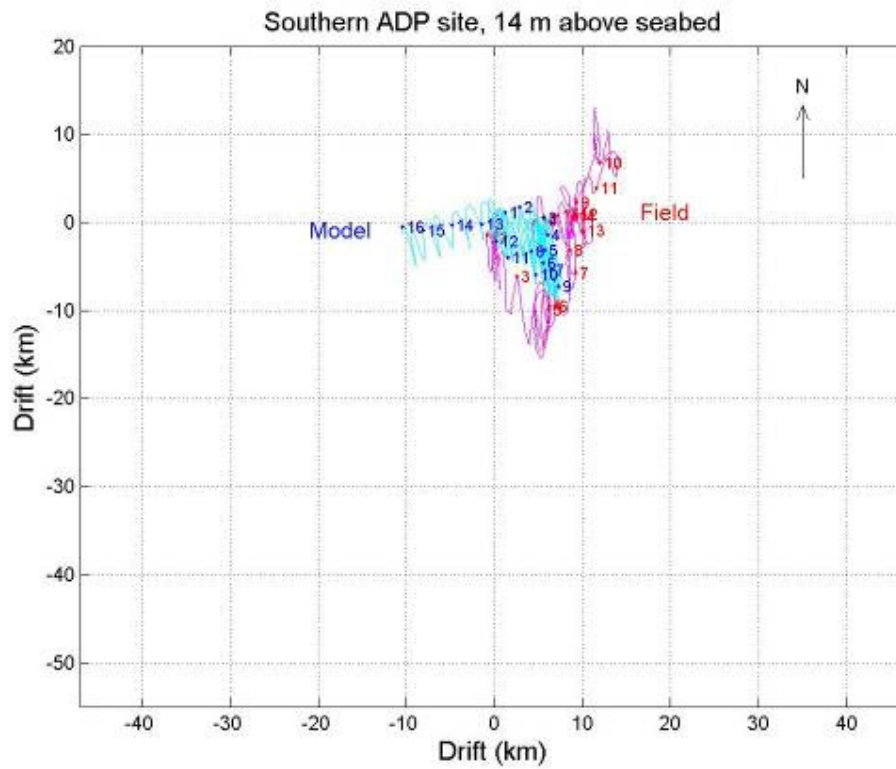
**Figure 17.**

Cumulative vector plot of current drift 2 m above the seabed at the *northern* ADP site. Both measured and modelled drift paths start at 0, 0. Red = measured by ADP, blue = simulated by model. Numbers 1–16 mark days since ADP deployment. North arrow indicates True North. North arrow indicates True North.
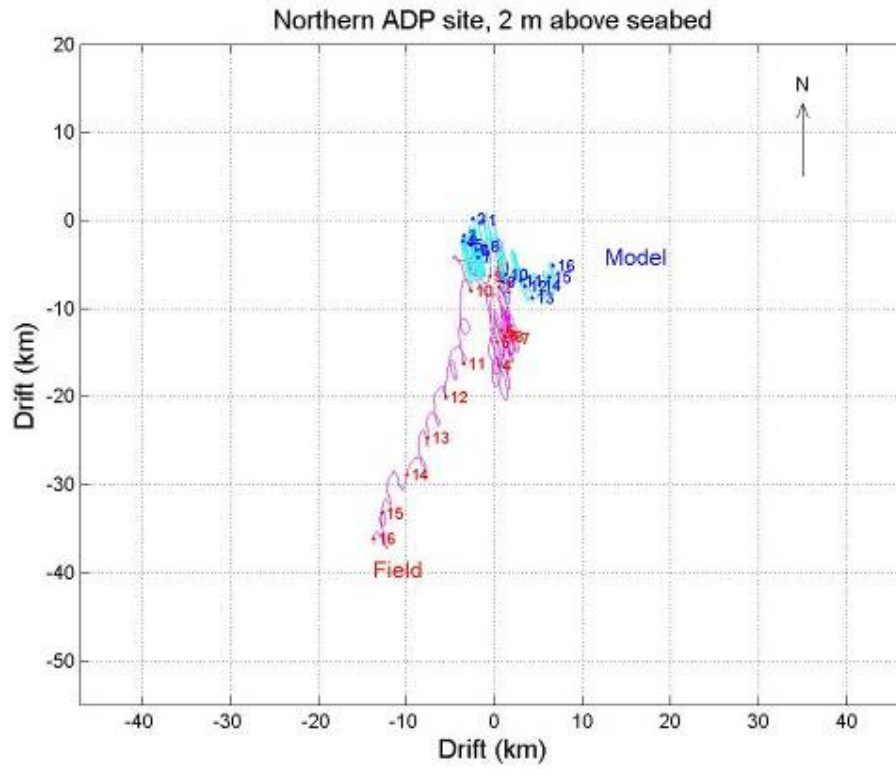
**Figure 18.**

Cumulative vector plot of current drift 12 m above the seabed (near surface) at the *northern* ADP site. Both measured and modelled drift paths start at 0, 0. Red = measured by ADP, blue = simulated by model. Numbers 1–16 mark days since ADP deployment.  North arrow indicates True North.
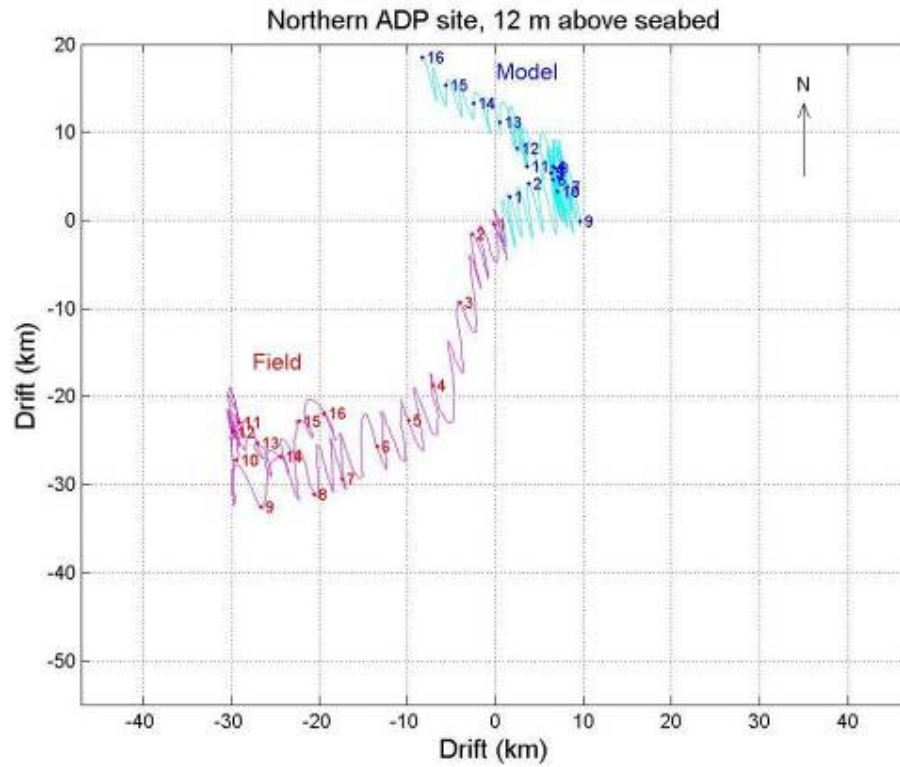
# 5 Conclusions

At the Waimangu Point site tidal currents account for 77% of the observed north-south currents with the remaining 23% being due to non-tidal residual currents. For the east-west component of observed currents 60% are due to tidal currents and 40% due to non-tidal residual currents. Tidal currents in the east-west direction are generally around one-tenth of the magnitude of the north-south component.

The verification shows that the hydrodynamic model simulates tidal currents that match reasonably well with observations at Waimangu Point. At least 90% of the dominant north-south tidal component is accounted for with the model. The model accounts for between 10 and 50% of the variation of the east-west component of the tidal current. Peak tidal currents are predicted to occur within less than 17 minutes of observed peak tidal currents and the direction of the peak flows are predicted to be within 2-10 ° of the observed peak flow direction.

The model predicts the depth-averaged temperature and salinity reasonably well but The variation of stratification with depth is not well represented in the model in the vicinity of Waimangu Point. Various changes to the constraints on the vertical dispersion of momentum, heat and salinity, along with changes to the horizontal dispersion could not improve the match to the measured stratification. To re-create the measurements may require the use of a different vertical-mixing scheme in the model, and subsequent re-calibration, or it may simply be that the forcing data supplied to the model is insufficient, e.g., no Waimangu Stream source and the paucity of Gulf temperature and salinity data for the open-sea boundary condition and setting the initial conditions in the Gulf and Firth.

Broekhuizen et al. (2005) suggested that the vertical dispersion might be too high in the model as originally calibrated. Our present familiarity with the model suggests that this is possibly the case, but the same lowering of the upper limits to vertical dispersion as suggested by Broekhuizen et al. (2005) did not improve the verification results presented here. Stratification in the model is sensitive to input parameters too and the appropriate forcing data for input to the hydrodynamic model was extremely limited, such as air temperature and relative humidity that control ocean-atmosphere heat-exchange.

Several factors suggest that the model is also not accurately reproducing the residual (non-tidal) currents at the Waimangu Point site:

- The model is unlikely to accurately reproduce vertically sheared flow in the absence of accurate stratification.

- At the southern site there is a reasonable good match between the current components near the sea-bed.  The model generally over-predicts the north-south component near the surface, while under-predicting the magnitude of the east-west component.

- Cumulative drift is poorly reproduced at the northern ADP comparison site with the model under-predicting the magnitude of the cumulative drift over the period of the verification.

The poor cumulative drift comparisons at the surface suggest that the input wind fields may not be accurate, but this could also result directly from lack of stratification in the model at this site or may reflect the relative spatial scale of changes in currents in the area compared to the model resolution of 750 x 750 m cells. As presently calculated, surface winds are only estimates interpolated from land-based stations spaced around the Firth of Thames, but is expected to provide a reasonable estimate of the general wind flow pattern over the outer Firth. However there will be localised topographic wind effects, particularly near land (e.g., at the Waimangu comparison sites) and localised wind patterns that affect the measurements at each wind station. One solution is to make sea-based wind measurements as part of a coordinated field programme or set up a wind model where local topographic steering is determined.

There has been no coordinated field data gathering exercise designed to calibrate and verify a three-dimensional hydrodynamic model over the entire Firth. Our opinion is that further effort into hydrodynamic modelling of the Firth of Thames is not warranted unless a substantial and specifically-targeted field programme is designed to provide the necessary database. The calibration (Stephens 2003), this verification and that of (Broekhuizen et al. 2005) have been undertaken using limited datasets at a few locations, and the model provided a reasonable match given the data limitations. Caution must be exercised when interpreting this verification because of the very spatially localised area of comparison. There may be localised influences such as peculiarities in the bathymetry near current meters, inaccurate specification of poorly documented river sources, and topographic influences on the wind at sites close to land that a large-scale model at 750 x 750 m resolution cannot be expected to reproduce, despite performing well on average over much of the domain. An example is the cumulative drift comparisons, where there was reasonable agreement throughout most of the water column at the southern site, but not at the northern site.

The key outcome of this body of work is to determine the ecological sustainability of large-scale aquaculture in the Firth. The simulation models of plankton dynamics are driven by output from the hydrodynamic model. Before further extensive work is undertaken on improving the hydrodynamic model, a key question that needs to be addressed is:

"How sensitive to hydrodynamics are the forecasts generated by the biological models?".

This report outlines the verification of the calibrated hydrodynamic model of the Firth of Thames and has identified some short comings of the model in terms of its ability to predict residual currents based on a comparison at 2 sites. If the hydrodynamic model were to be improved further, it is not clear how sensitive the biological models would prove to be the comparatively subtle hydrodynamic changes that would arise.

Without running further simulations in which we introduce subtle changes in the hydrodynamics (rather than the dramatic ones considered in Broekhuizen et al. 2005), we can only speculate on this issue. For example, how would improvements to the

hydrodynamics effect the magnitude of within-farm depletion and how would the direction and spatial extent of any farm-induced plankton 'halo' change?

The magnitude of within-farm depletion is determined by a combination of the farm's stocking characteristics, the rate at which water moves through the farm, and to a lesser extent, the growth rate of the plankton. The first of these is unaffected by simulated hydrodynamics. For small farms, the tidal excursion[2] will exceed the farm dimensions. In this case tidal currents (which are predicted reasonably well by the model) may dominate the (horizontal) flushing rate. For large farms, it will be a combination of tidal excursion and the residual (non-tidal) currents which determine the (horizontal) flushing rate.

We believe the following statements about local-scale plankton change are broadly justified:

1) Where the residual drift velocity and direction are well simulated, forecasts of plankton change will be robust.

2) Where the residual drift velocity is well simulated, but the residual drift direction is incorrect, we also anticipate that forecasts of plankton change will be robust – unless the farm is 'long-and-narrow' (such that any error in the direction of the tidal and/or residual currents dramatically changes the farm's flushing time).

3) Where the simulated residual velocities are too low, the biological models' forecasts of farm-induced local-scale plankton change may be too large (i.e., overly conservative). Despite this, it is possible that the far-field footprint may be under-estimated.

4) Conversely, where the simulated residual velocities are too large, the biological models will under-predict local-scale farm-induced plankton change.

To date, we have considered a large AMA in the western Firth. It does not have an extreme aspect ratio (is not exceptionally long and thin). This suggests that direction-errors identified during the verification process will have little influence upon estimates of farm-scale plankton change.

At the two Waimangu Point sites the model tends to under-predict the non-tidal currents (especially near the sea-surface). We suggest that the subtle changes in hydrodynamics resulting from an improved calibration of the hydrodynamic model may lead to lower predictions of plankton at a local-scale. Improvements to the hydrodynamic model will influence the instantaneous location of far-field farm-influences, but we suspect that when averaged over periods of weeks-to-months, the resultant time-averaged footprints would not be extremely sensitive to the observed scale of discrepancy between observed and simulated residual currents. Residual flows are driven by winds which occur from all directions (with the dominant wind direction being south-west). Thus, even if the model fails to reproduce the exact location of the 'instantaneous foot-print', it is much more likely to sweep out an appropriate 'long-term, time-averaged foot-print' – provided that the <u>magnitudes</u> of residual currents are adequately reproduced. If the magnitudes are consistently too

---

[2] The total drift distance on an ebb or flood tide.

high, one might expect that the time-averaged footprints would extend over an excessively large area. However this might not occur because there would also be less change at the source (farm), so the plankton would need less time to recover. Conversely, whilst one might expect the extent of the footprint to be under-predicted if the forecast residual velocities are consistently too low, this will be offset by greater local-scale change.

The proposed environmental standards that will govern farm operations are presented in terms of annual-scale average change, and whilst they stipulate how much change is permitted within the AMA, and how much change is permitted at the Firth-scale, they make no stipulations as to exactly where any far-field change can/cannot be permitted. Thus, we believe that consideration of the ensemble results from the six different hydrodynamic scenarios previously considered will certainly provide a useful guide as to the likely magnitude of local-scale and Firth-scale magnitudes of change. We acknowledge that there is a possibility that the precise geographic location of a particular isocline of change (for example 5% depletion) might be less well simulated, but we believe that the results will provide a useful guide for developing environmental standards in lieu of embarking on an extensive field programme and undertaking modelling on a higher resolution grid.

This report presents a verification of the Firth of Thames hydrodynamic model. The hydrodynamic model was developed to predict physical conditions in the Firth, so that, when coupled with a biological model, predictions could be made about the extent of plankton depletion resulting from different scales of development of mussel farming. The verification described in this report revealed some deficiencies in the hydrodynamic model. The implications of this were explored in a separate piece of work for Environment Waikato, in which the sensitivity of the plankton models to hydrodynamic forcing were investigated. Results from this sensitivity analysis are presented as Addendum 1 to this report.

# 6  References

Broekhuizen, N.; Ren, J.; Zeldis, J.; Stephens, S. (2004). Ecological sustainability assessment for Firth of Thames aquaculture: Tasks 2-4 - Biological modelling. NIWA Consultancy Report HAM2003-120 prepared for Auckland Regional Council, Environment Waikato and Western Firth Consortium. 62 p.

Broekhuizen, N.; Zeldis, J. (2005). Forecasts of possible phytoplankton responses to elevated riverine nitrogen delivery into the southern Firth of Thames. *No.* HAM2005-131. 50 p.

Broekhuizen, N.; Oldman, J.; Image, K.; Gall, M.; Zeldis, J. (2005). Verification of plankton depletion models against the Wilson Bay synoptic survey data. NIWA Consulting Report HAM2005-002 prepared for the Auckland Regional Council. 66 p.

Hadfield, M.; Uddstrom, M.; Goring, D.; Gorman, R.; Wild, M.; Stephens, S.; Shankar, U.; Niven, K.; Snelder, T. (2002). Physical variables for the New Zealand Marine Environment Classification System: development and description of data layers. NIWA Consulting Report CHC2002-043 prepared for the Ministry for Environment. 59 p.

Oldman, J.; Hong, J.; Stephens, S.; Broekhuizen, N. (2006). Verification of the Firth of Thames hydrodynamic model. *No.* HAM2005-127 (ARC05243). 69 p.

Stephens, S. (2003). Ecological sustainability assessment for Firth of Thames shellfish aquaculture: Task 1 – Hydrodynamic modelling. NIWA Consulting Report HAM2003-113 prepared for Auckland Regional Council, Environment Waikato and Western Firth Consortium. 32 p.

Turner, S.M.; Felsing, M. (2005). Trigger points for the Wilson's Bay marine farming zone. *Environment Waikato Technical Report No.* TR 2005/28. 30 p.

Walters, R.A.; Goring, D.G.; Bell, R.G. (2001). Ocean tides around New Zealand. *New Zealand Journal of Marine and Freshwater Research 35*: 567-579.

Zeldis, J.; Hayden, B.; Image, K.; Ren, J.; Hatton, S.; Gall, M. (2001). Assessment of sustainable production issues for a marine farm proposal in Firth of Thames (Waimangu Point). NIWA Consulting Report CHC01/44 prepared for Thames Mussels Limited. 37 p.

# 7 Appendix 1 – Time-series plots comparing measured and simulated currents

**Figure 19**.

Comparison between north-south current component 2 m above the seabed, measured at the northern ADP site and output from the model at from the nearest grid node.

**Figure 20**.

Comparison between north-south current component 4 m above the seabed, measured at the northern ADP site and output from the model at from the nearest grid node.

**Figure 21.**

Comparison between north-south current component 6 m above the seabed, measured at the
northern ADP site and output from the model at from the nearest grid node.

**Figure 22.**
Comparison between north-south current component 8 m above the seabed, measured at the northern ADP site and output from the model at from the nearest grid node.

**Figure 23**.

Comparison between north-south current component 10 m above the seabed, measured at the northern ADP site and output from the model at from the nearest grid node.

**Figure 24.**

Comparison between north-south current component 12 m above the seabed, measured at the northern ADP site and output from the model at from the nearest grid node.

**Figure 25.**

Comparison between north-south current component 2 m above the seabed, measured at the *southern* ADP site and output from the model at from the nearest grid node.

**Figure 26.**

Comparison between north-south current component 4 m above the seabed, measured at the *southern* ADP site and output from the model at from the nearest grid node.

**Figure 27.**

Comparison between north-south current component 6 m above the seabed, measured at the *southern* ADP site and output from the model at from the nearest grid node.

**Figure 28.**

Comparison between north-south current component 8 m above the seabed, measured at the *southern* ADP site and output from the model at from the nearest grid node.

**Figure 29.**

Comparison between north-south current component 10 m above the seabed, measured at the *southern* ADP site and output from the model at from the nearest grid node.

**Figure 30.**

Comparison between north-south current component 12 m above the seabed, measured at the
*southern* ADP site and output from the model at from the nearest grid node.

**Figure 31.**

Comparison between north-south current component 14 m above the seabed, measured at the *southern* ADP site and output from the model at from the nearest grid node.

**Figure 32.**

Comparison between east-west current component 2 m above the seabed, measured at the *northern* ADP site and output from the model at from the nearest grid node.
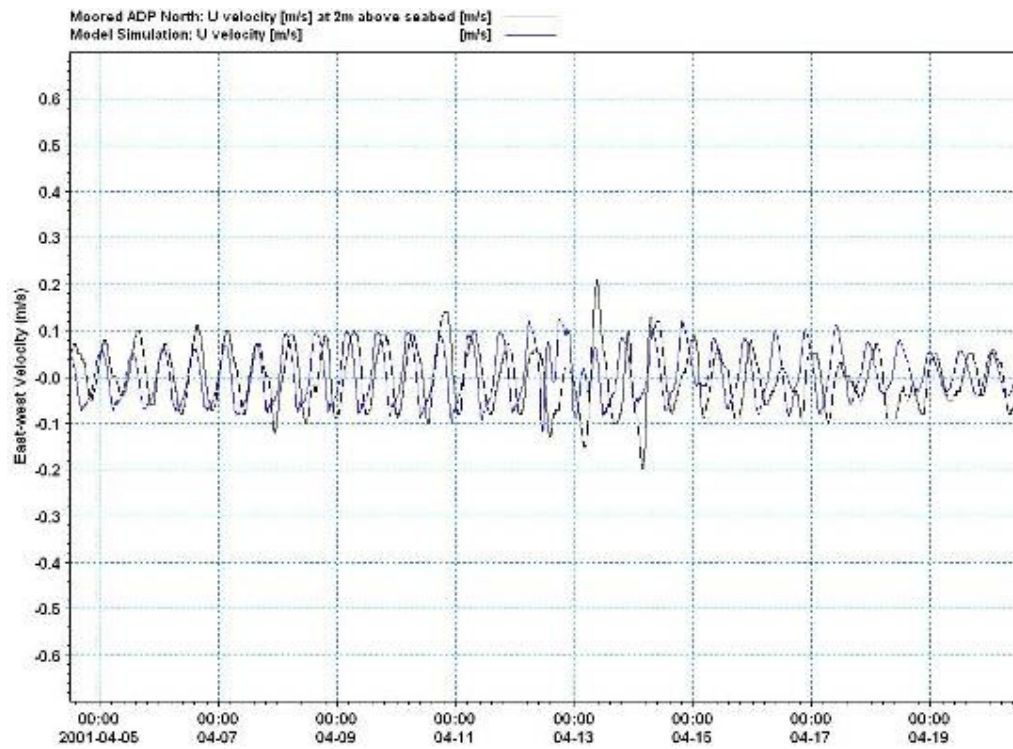
**Figure 33.**

Comparison between east-west current component 4 m above the seabed, measured at the *northern* ADP site and output from the model at from the nearest grid node.
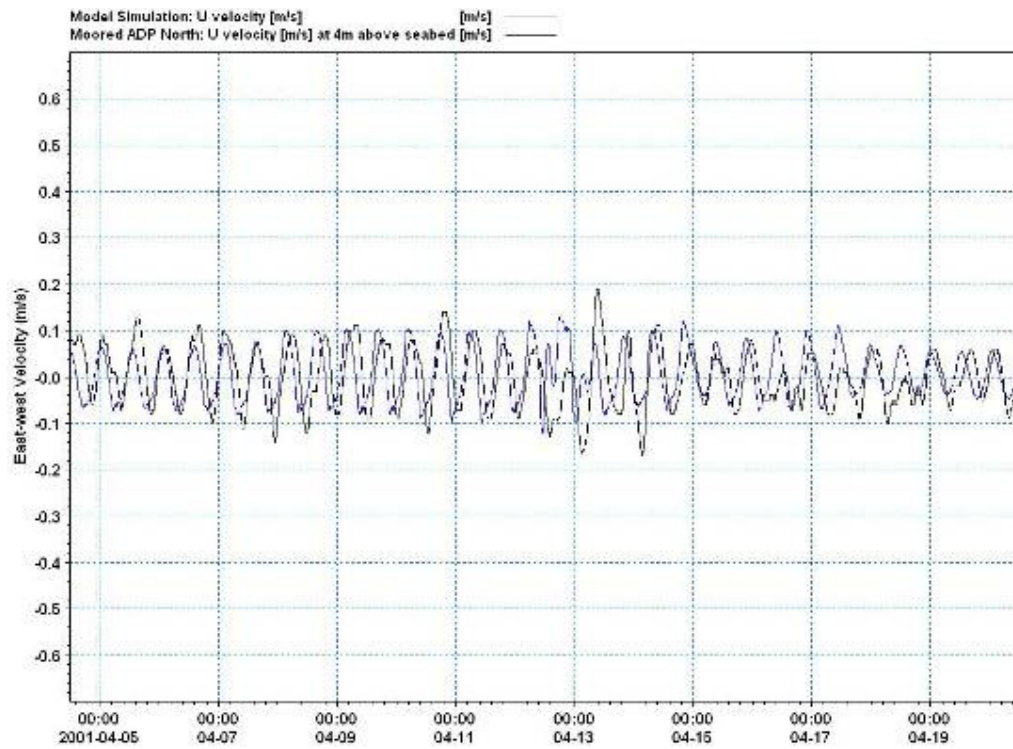
**Figure 34.**

Comparison between east-west current component 6 m above the seabed, measured at the *northern* ADP site and output from the model at from the nearest grid node.
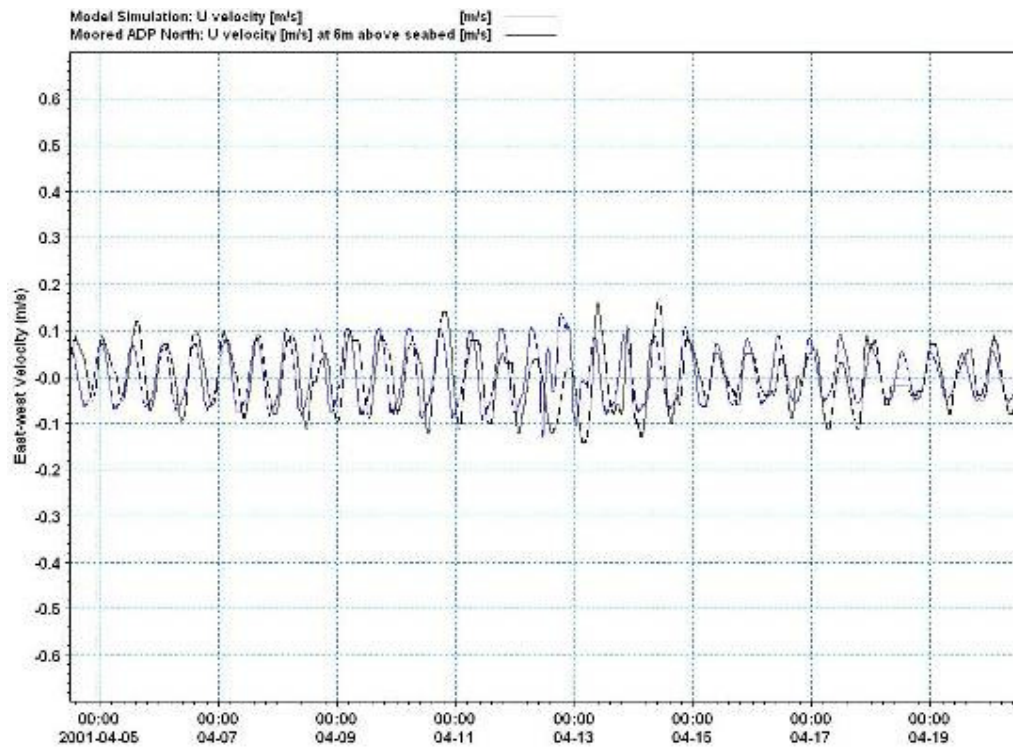
**Figure 35.**

Comparison between east-west current component 8 m above the seabed, measured at the *northern* ADP site and output from the model at from the nearest grid node.
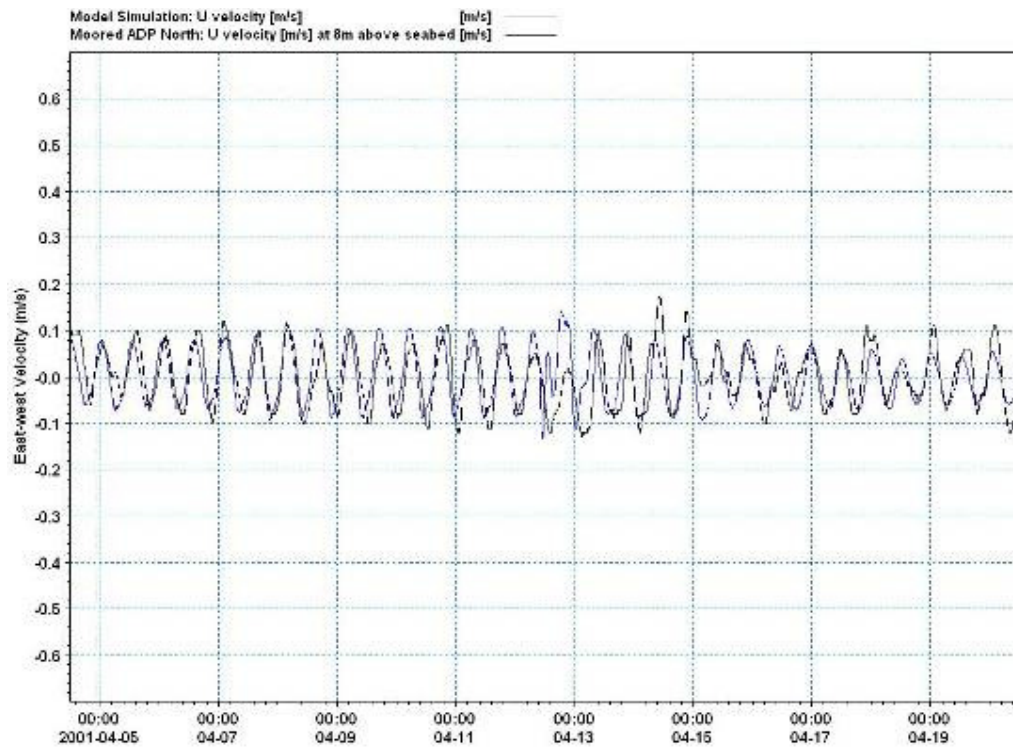
**Figure 36.**

Comparison between east-west current component 10 m above the seabed, measured at the *northern* ADP site and output from the model at from the nearest grid node.
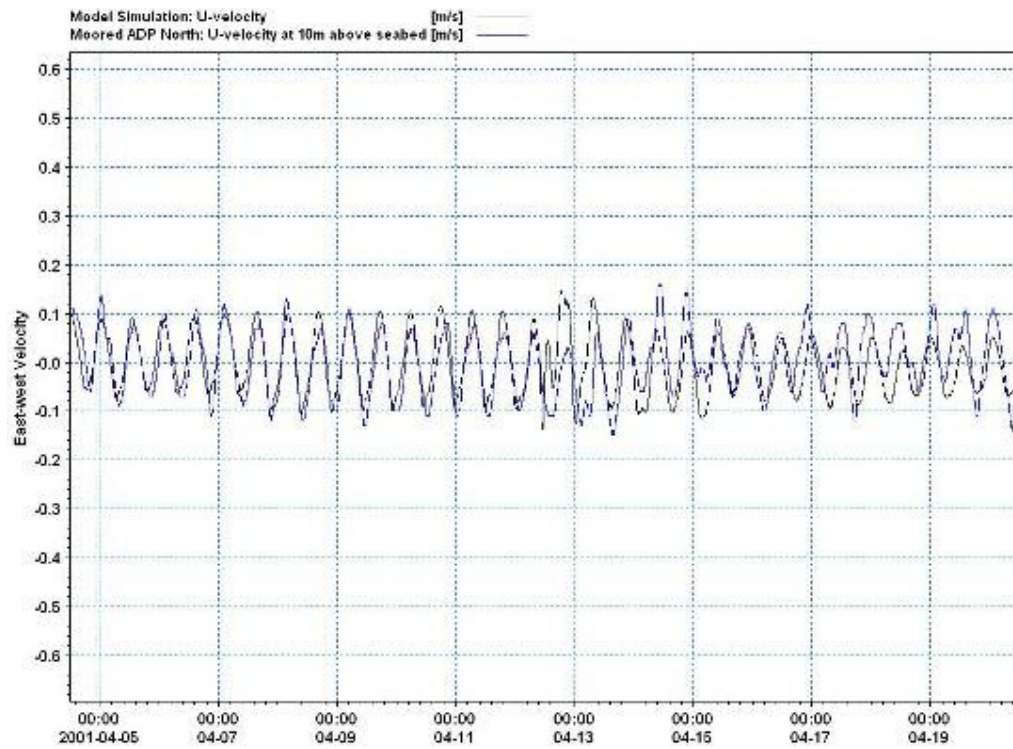
**Figure 37.**

Comparison between east-west current component 12 m above the seabed, measured at the *northern* ADP site and output from the model at from the nearest grid node.

**Figure 38.**

Comparison between east-west current component 2 m above the seabed, measured at the *southern* ADP site and output from the model at from the nearest grid node.

**Figure 39.**

Comparison between east-west current component 4 m above the seabed, measured at the *southern* ADP site and output from the model at from the nearest grid node.

**Figure 40.**

Comparison between east-west current component 6 m above the seabed, measured at the *southern* ADP site and output from the model at from the nearest grid node.

**Figure 41.**

Comparison between east-west current component 8 m above the seabed, measured at the *southern* ADP site and output from the model at from the nearest grid node.

**Figure 42.**

Comparison between east-west current component 10 m above the seabed, measured at the *southern* ADP site and output from the model at from the nearest grid node.

**Figure 43.**

Comparison between east-west current component 12 m above the seabed, measured at the *southern* ADP site and output from the model at from the nearest grid node.

**Figure 44.**

Comparison between east-west current component 14 m above the seabed, measured at the
*southern* ADP site and output from the model at from the nearest grid node.

# 8 Appendix 2 – cumulative vector plots

**Figure 45.**

Cumulative vector plot of current drift 4 m above the seabed at the southern ADP site. Both measured and modelled drift paths start at 0, 0. Red = measured by ADP, blue = simulated by model. Numbers 1–16 mark days since ADP deployment. North arrow indicates True North.
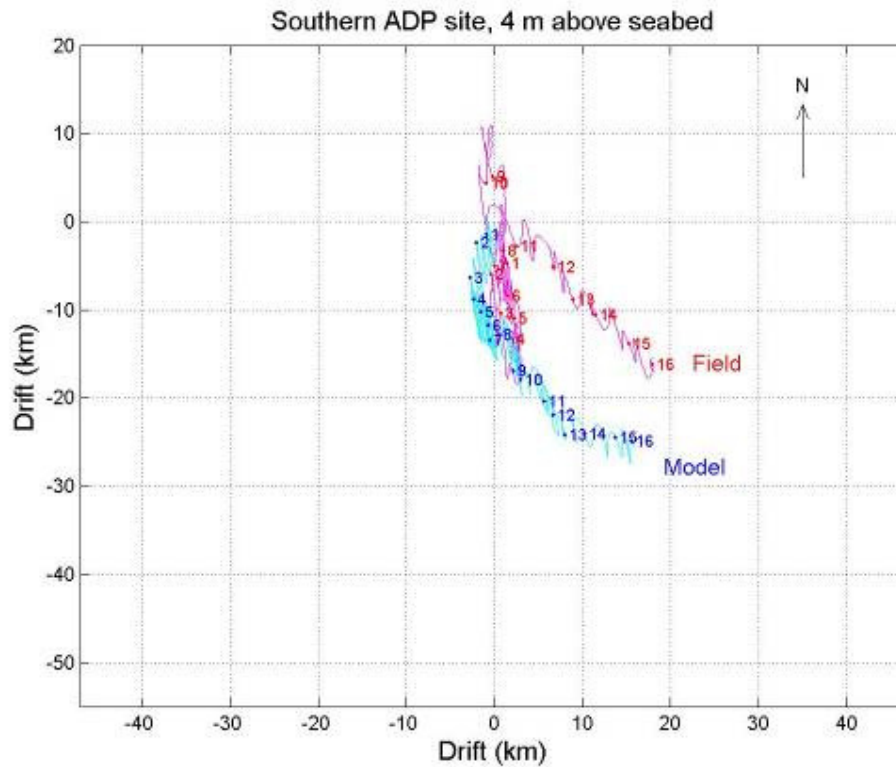
**Figure 46.**

Cumulative vector plot of current drift 6 m above the seabed at the southern ADP site. Both measured and modelled drift paths start at 0, 0. Red = measured by ADP, blue = simulated by model. Numbers 1–16 mark days since ADP deployment. North arrow indicates True North.
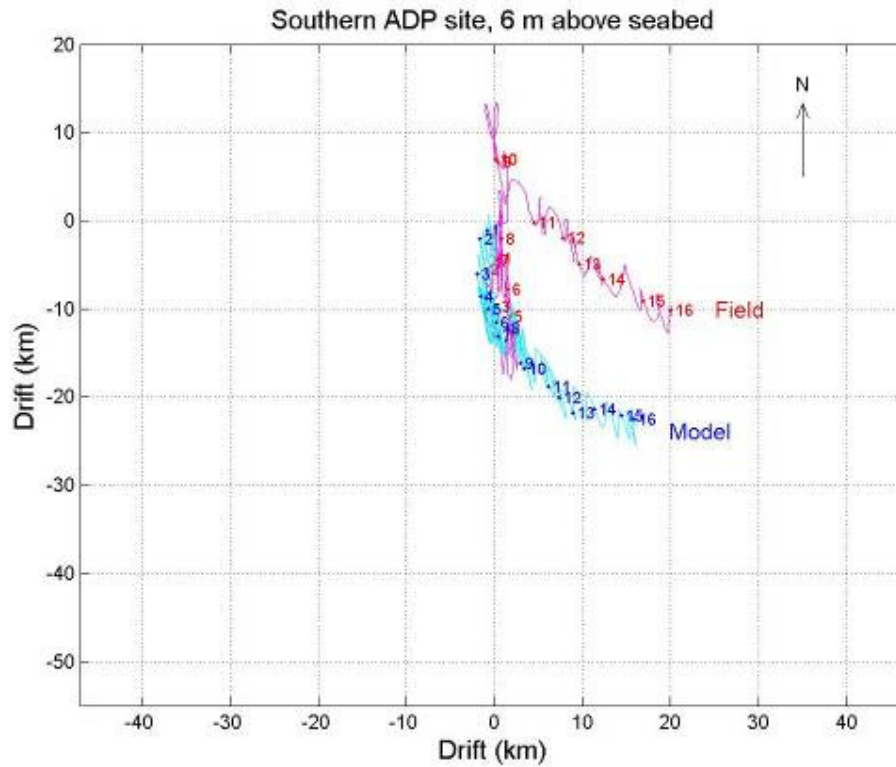
**Figure 47.**

Cumulative vector plot of current drift 8 m above the seabed at the southern ADP site. Both measured and modelled drift paths start at 0, 0. Red = measured by ADP, blue = simulated by model. Numbers 1–16 mark days since ADP deployment. North arrow indicates True North.
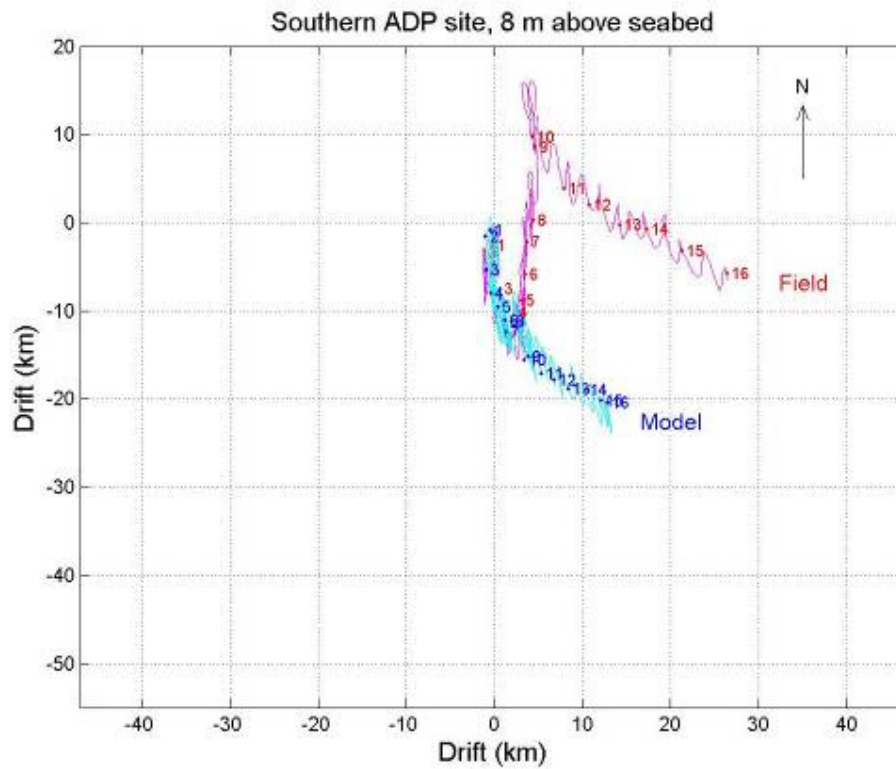
**Figure 48.**

Cumulative vector plot of current drift 10 m above the seabed at the southern ADP site. Both measured and modelled drift paths start at 0, 0. Red = measured by ADP, blue = simulated by model. Numbers 1–16 mark days since ADP deployment.  North arrow indicates True North.
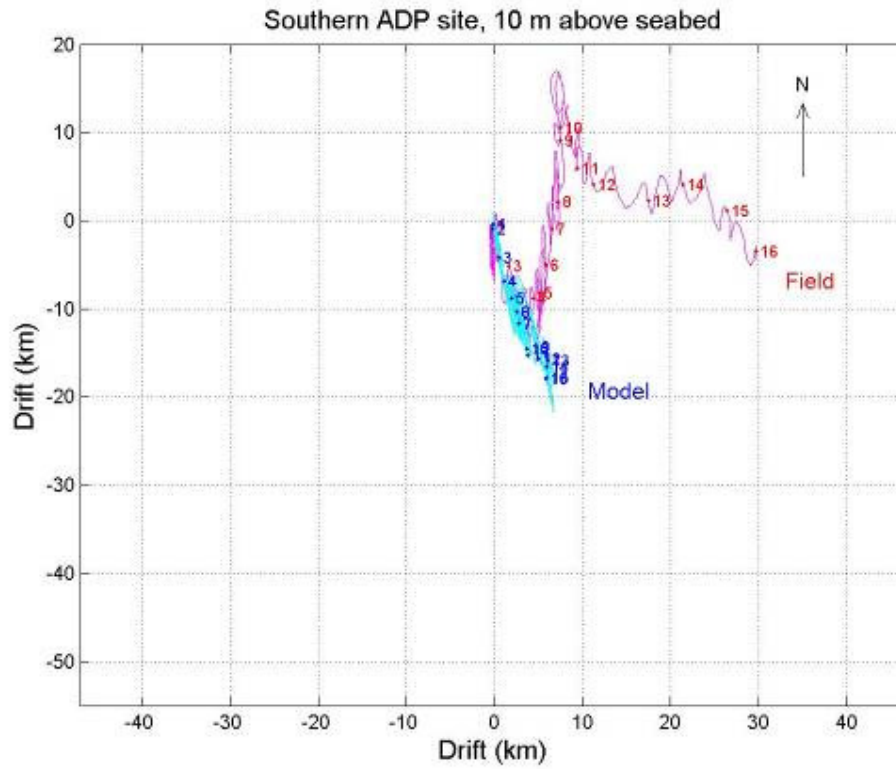
**Figure 49.**

Cumulative vector plot of current drift 12 m above the seabed at the southern ADP site. Both measured and modelled drift paths start at 0, 0. Red = measured by ADP, blue = simulated by model. Numbers 1–16 mark days since ADP deployment.  North arrow indicates True North.
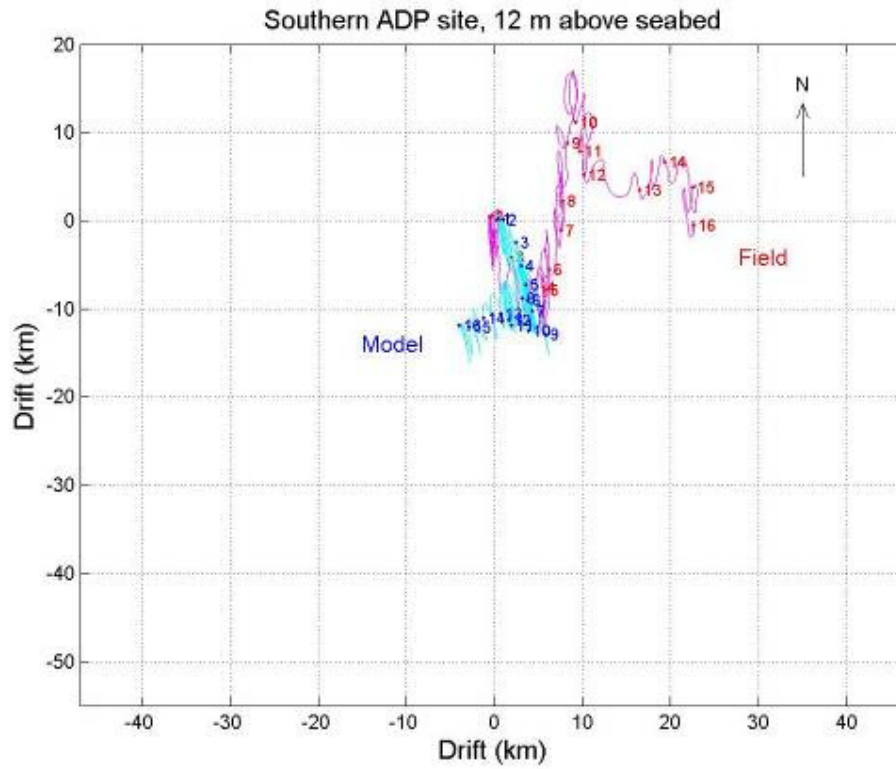
**Figure 50.**

Cumulative vector plot of current drift 4 m above the seabed at the *northern* ADP site. Both measured and modelled drift paths start at 0, 0. Red = measured by ADP, blue = simulated by model. Numbers 1–16 mark days since ADP deployment.  North arrow indicates True North.
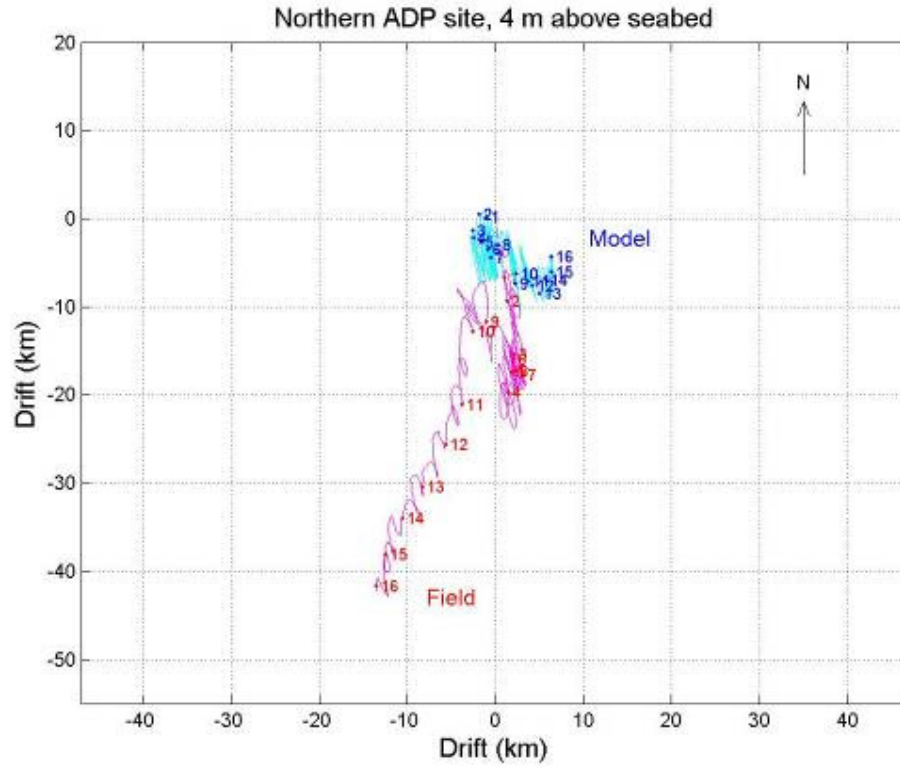
**Figure 51.**

Cumulative vector plot of current drift 6 m above the seabed at the *northern* ADP site. Both measured and modelled drift paths start at 0, 0. Red = measured by ADP, blue = simulated by model. Numbers 1–16 mark days since ADP deployment. North arrow indicates True North.
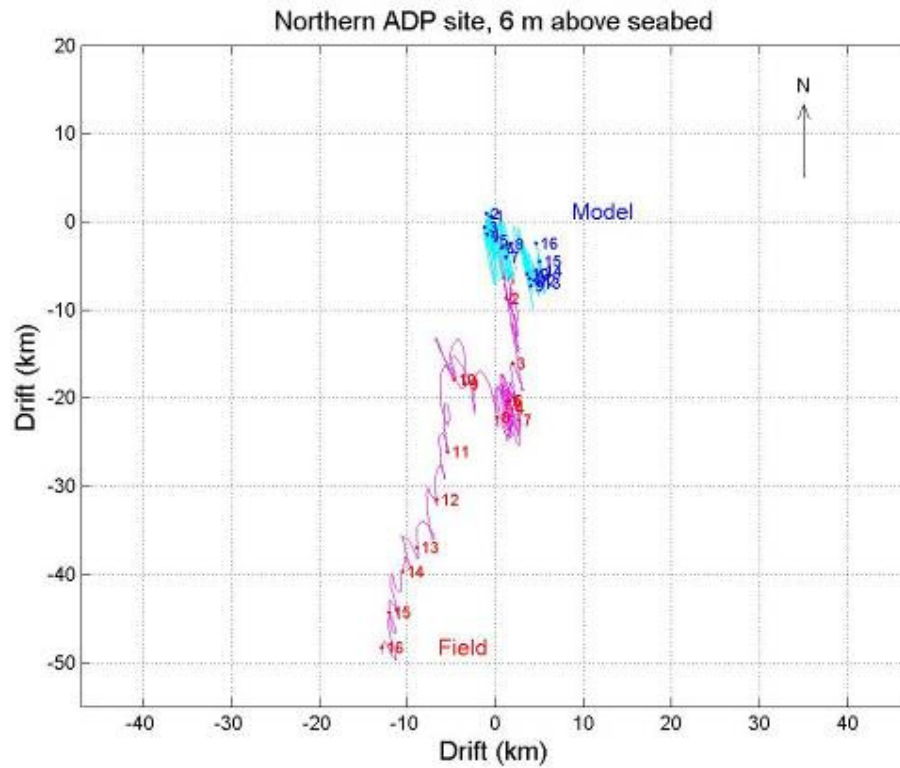
**Figure 52.**

Cumulative vector plot of current drift 8 m above the seabed at the *northern* ADP site. Both measured and modelled drift paths start at 0, 0. Red = measured by ADP, blue = simulated by model. Numbers 1–16 mark days since ADP deployment.  North arrow indicates True North.
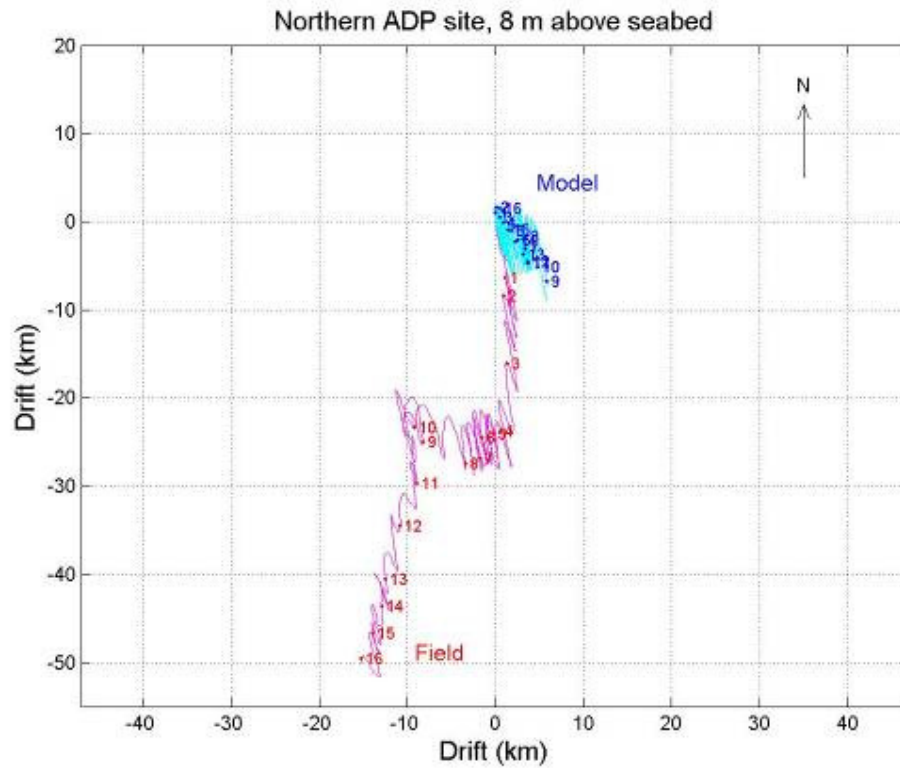
**Figure 53.**

Cumulative vector plot of current drift 10 m above the seabed at the *northern* ADP site. Both measured and modelled drift paths start at 0, 0. Red = measured by ADP, blue = simulated by model. Numbers 1–16 mark days since ADP deployment.  North arrow indicates True North.
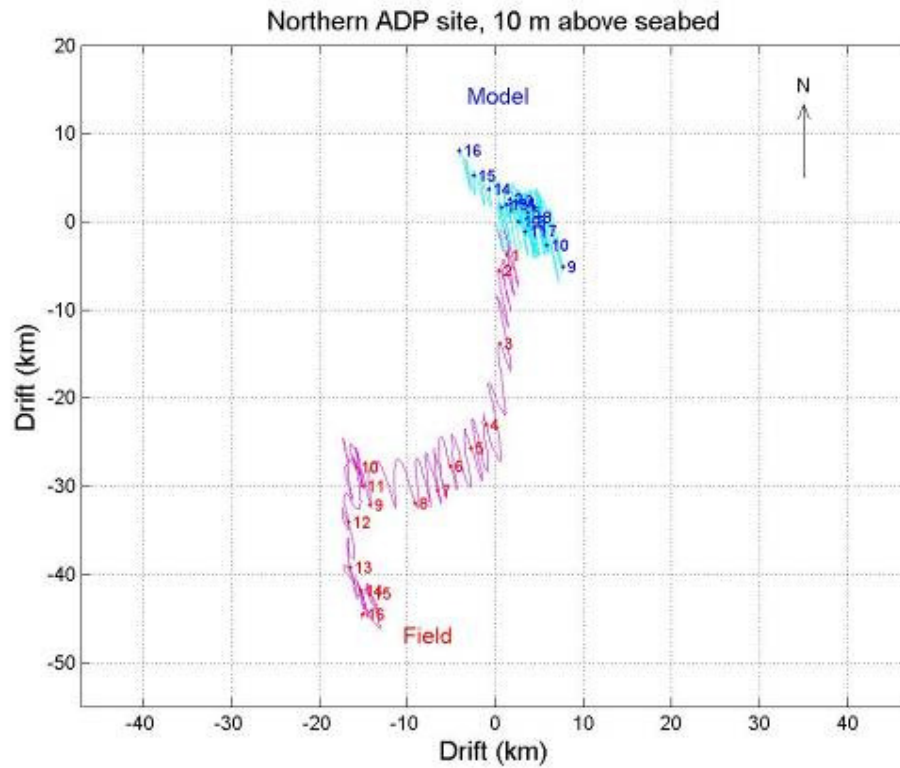
# 9    Addendum 1

Interpretation of simulated mussel-farm induced modification
of the plankton community relative to the Limits of Acceptable
Change criteria: sensitivity to hydrodynamic forcing

N. Broekhuizen

# Executive Summary

There has been a large body of work related to numerical simulation of the influences of aquaculture in the Firth of Thames (Stephens & Broekhuizen (2003), Broekhuizen et al. (2004), Broekhuizen et al. (2005) and Oldman et al. (2006)). The early work was made using unverified models. The two latter reports present results from a verification analysis. The verification identified, and rectified some discrepancies between the observed and simulated patterns of plankton change beyond the perimeter of the Wilson Bay Area A farm (see Appendix of Broekhuizen et al. (2005)). The verification also revealed some deficiencies in the performance of the hydrodynamic model. In particular, it does not always fully reproduce the vertical distribution of temperature and salinity in the water-column, and whilst the tidal currents are well reproduced, the simulated longer-term residuals are not always of the right magnitude or direction. Inevitably, this leads one to question whether conclusions drawn from subsequent biological modelling (which uses output from the hydrodynamic model) are robust.

Environment Waikato asked NIWA to address the robustness of the conclusions drawn from the biological model. This report is the outcome. Its content draws heavily upon work that has been funded by New Zealand's Foundation for Research and Science and Technology through NIWA's Sustainable Aquaculture Program (contract CO1X0507).

We argue that, when interpreted through the *Limits of Acceptable Change Criteria* (LAC, against which it has been agreed that the environmental effects of aquaculture in the Firth of Thames should be measured), the results from the biological modelling are not sensitive to discrepancies between observed and simulated hydrodynamics. There are two reasons for this. Firstly, the magnitude of simulated depletion is small (well below that permitted by the LAC, and similar to that inferred from field data). Secondly, the LAC criteria make no stipulations regarding where (within the Firth) any plankton downstream changes in the plankton community may occur. Thus, errors in the direction of residual currents are of little importance. We present new simulation results and new analyses supporting these arguments.

Whilst the conclusions drawn from the biological modelling are robust when interpreted through the LAC-criterion, it is important to understand that the location of any far-field change in the plankton community is sensitive to the hydrodynamics. It is clear that the performance of the hydrodynamic model will need to be improved before it (or models depending upon it) can be applied to questions concerning location-specific downstream effects.

# <sub>1.1</sub> Introduction

There has been a large body of work related to numerical simulation of the influences of aquaculture in the Firth of Thames (Stephens & Broekhuizen (2003), Broekhuizen et al. (2004), Broekhuizen et al. (2005) and Oldman et al. (2006)). The original intent of the body of work was to infer the magnitude and location of change (in the plankton community) that might be induced by large-scale aquaculture in the Firth of Thames. To do so, we used spatially resolved models of plankton dynamics (incorporating the influence of mussel farms upon plankton demography). The models were driven with simulated hydrodynamic conditions stemming from an implementation of the DHI MIKE3 model. Initially, there were few data against which to verify the performance of either the hydrodynamic model, or the biological model. Since the initial work began, additional information has become available, and the scope of the project has changed:

Firstly, a limited amount of data has become available to permit verification of both the hydrodynamic and biophysical models (Broekhuizen et al. (2005), Oldman et al. (2006)). Secondly, a set of Environmental Standards (the so-called *Limits of Acceptable Change* (henceforth, LAC), Turner & Felsing 2005) has been negotiated. Any impacts of shellfish aquaculture activities associated with the Wilson Bay Marine Farming zone are to be judged against these standards. Thirdly, Auckland Regional Council has delayed its decision regarding notification of an Aquaculture Management Area (AMA) in the western Firth of Thames. For the time-being, this implies that the results from the plankton modelling will be used only in terms of assessing the possible environmental effects of already-mandated mussel farming areas (principally, Wilson Bay Areas A and B, the former already occupied, the latter not yet occupied).

Two earlier verification reports (Broekhuizen et al. (2005) and Oldman et al. (2006)) have revealed that whilst the hydrodynamic model reproduces tidal signals well, it does not always reproduce the longer-term, residual circulation patterns so well and can fail to fully reproduce the patterns of vertical stratification. Inevitably, this leads one to question whether conclusions drawn from subsequent biological modelling are robust. It is our opinion that they are – given the manner in which the results will be interpreted. We will provide more detailed support for this argument in sections 2 & 3 below, but in summary:

the environmental standards (LAC-criteria) governing farm-induced change in the plankton community stipulate only farm-scale and Firth-scale thresholds. There are no stipulations concerning impacts <u>at a particular location</u> within the Firth (other than within the immediate vicinity of the farm). Thus, the direction of any residual current is comparatively unimportant.

we previously made simulations for a variety of wind/season combinations. These caused residual circulation patterns, which differ from one another to a much greater degree than the discrepancies between observation and simulation that have been identified. These radically different circulation patterns were used to drive subsequent simulations with the biological models. It transpires that, <u>when interpreted relative to the LAC-criteria</u>, inferences drawn from the results of the biological model are <u>insensitive to the residual circulation patterns</u> (note, we are not arguing that the raw model results from the biological modelling are insensitive to the circulation patterns).

Verification of Firth of Thames hydrodynamic model - Addendum - Interpretation of simulated mussel-farm induced modification of the plankton community relative to the Limits of Acceptable Change criteria: sensitivity of hydrodynamic forcing

72

# 12 Analytical studies

Of the various environmental standards that have been agreed for the Wilson Bay Marine Farming zone, two apply to plankton (page 13 of Turner & Felsing (2005)). One states that, *spatially and temporally averaged chlorophyll depletion shall not exceed 25% within an area equal to [3] twice the area of the Wilson Bay marine farming zone.* The other states that, *spatially and temporally averaged chlorophyll depletion shall not exceed 20% over more than 10% of the Firth.* Whilst not stated explicitly, it is our understanding that these criteria apply to annual averages rather than shorter-term averages.

At the farm-scale, the dominant determinants of depletion are: (a) mussel stocking practices, (b) residence time of a parcel of water during each passage through the farm, (c) the number of passages which the water-parcel makes through the farm before residual currents eventually imply that it will not re-enter the farm again, and (d) the net growth rate of the plankton.

Of these four factors, (a) is assumed to be well known and (b) is dictated by the tidal velocities (which the model is reproducing well). Where residual current speeds (cf direction) are high, the remaining two factors have negligible importance (with respect to determining within-farm depletion). Where residual current speeds are low, (c) and (d) become relatively more important.

The spatial extent (cf location) of the far-field (i.e., beyond the radius of the tidal excursion around a farm's perimeter) change-plume induced by a farm is influenced by three factors: (i) the magnitude of change evident in a water-parcel when it departs the farm for the last time, (ii) the rapidity with which this parcel mixes with water that has never passed through a farm, and (iii) the net growth rate of the residual plankton community within the parcel. The instantaneous location of the plume is dictated by the direction of the residual currents as well as their speed, and the plankton net growth rate.

We will now develop an analytical, quantitative expression to predict the magnitude of depletion at a farm's downstream perimeter, and the downstream radius of the plume of depleted water. The analytical model is sufficiently simply that it can be used to give a qualitative insight into the key processes governing the pattern of plankton change around the system. Thus, it serves a useful didactic purpose.

In order to develop the analytical expression, we must make some simplifying assumptions. Thus, in a subsequent section we show results from a second model. That model incorporates ore mechanistic detail, but cannot be solved analytically. Instead it is solved by numerical integration. Results from the two models complement one another.

We assume that, in the absence of farms, plankton dynamics can be represented by the logistic growth equation, and that when within a farm, the plankton suffer an

---

[3] Twice the are of the Wilson Bay marine farming zone amounts to approximately 5.6% of the total area of the Firth (Turner & Felsings (2005)).

additional first-order mortality (i.e., the mussels remove a fixed proportion of the plankton per unit time – this amounts to assuming that the mussels do not change their pumping rates and filtration efficiencies in response to changes in plankton abundance, and that the vulnerability of the surviving plankton does not change with time or position in the farm).  Thus, the instantaneous rate of change of plankton abundance is given by:

$$\frac{dN}{dt} = rN\left(1 - \frac{N}{K}\right) - f(\text{location})N = (r - f(\text{location}))N - \frac{r}{K}N^2 \qquad (1)$$

In which $N$ denotes plankton concentration, $r$ denotes the maximum mass-specific net growth rate of the plankton, $K$ denotes the 'carrying capacity' (equilibrium concentration to which the plankton population will grow <u>in the absence of farms; note the implicit assumption that this is spatially and temporally invariant</u>) and $f(\text{location})$ is the plankton-mass-specific mortality induced by the mussel-crop.  This is zero outside the farm's perimeter and exceeds zero within the farm.

Equation (1) has an analytical solution:

$$N(t) = \frac{(r - f)N_0 K}{K(r - f)e^{-(r-f)t} - re^{-(r-f)t}N_0 + rN_0} \qquad (2)$$

In which $N_0$ denotes the starting population. Let us now consider the evolution of a plankton population as it passes through, and beyond a farm.  Let us assume that the population enters the farm at its carrying capacity, that the water velocity is $v$ m s$^{-1}$, and that in the direction of the water-velocity, the farm is a distance $\Delta x$ m long.  Whilst within the farm, the population evolves according to Eq. (2), with $N_0 = K$ and $f > 0$.  It takes a time

$$t_{passage} = \frac{\Delta x}{v} \quad \text{to pass between the upstream and downstream perimeters of the farm.}$$

Thus, at the downstream perimeter of the farm, the plankton concentration is given by:

$$N(t_{passage}) = \frac{(r - f)K^2}{K(r - f)e^{-(r-f)t_{passage}} - Kre^{-(r-f)t_{passage}} + rK} \qquad (3)$$

Thereafter, the population evolves according to Eq. (2), but with $N_0 = N(t_{passage})$ and $f = 0$ (i.e., it evolves according to the standard logistic equation).  Upon exit from the farm, the population will start returning towards its carrying capacity (provided $r > 0$) – however it approaches that abundance only asymptotically.  Thus, it would take infinite time to fully recover. We can, however ask: '*how long will it take a population to return to within some fraction ($\alpha$ $(0 \le \alpha < 1)$ of the carrying-capacity, and how far downstream has it travelled in that time?* We can answer the first of these questions by making the substitution $N(t) = \alpha K$ , $f = 0$ and $N_0 = N(t_{passage})$ in equation (1), and then rearranging it to solve for time (t).  The downstream travel-distance is easily

derived as the product of this time and the water velocity ($v$). Thus, we wish to find $t$ such that:

$$\alpha K = \frac{rN(t_{passage})K}{Kre^{-r(t-t_{passage})} - re^{-r(t-t_{passage})}N(t_{passage}) + rN(t_{passage})} \tag{4}$$

The solution is:

$$t = -t_{passage} - \frac{1}{r}\ln\left(\frac{(1-\alpha)N(t_{passage})}{\alpha(K - N(t_{passage}))}\right) \tag{5}$$

These expressions make it possible to derive estimates: (a) depletion at the downstream edge of the farm, and (b) the length of the 'recovery radius' as a function of water velocity. Examples are provided in Figures 1 a-d. It should come as no surprise that the magnitude of depletion at the downstream end of the farm increases as the water velocity falls. This explanation is obvious: the plankton have been resident within the farm for longer and have therefore been exposed to mussel grazing for longer. It is, perhaps a little more surprising that the radius of the downstream plume is dependent upon the manner in which recovery is defined (i.e., the value of $\alpha$, see Eq. 4). When $\alpha$ is large, the radius of the downstream plume increases monotonically (albeit in a sub-linear manner). When $\alpha$ is smaller, the recovery radius is small at small and large water velocities, and large at intermediate velocities. The reason is as follows. Within the logistic model, it is implicit that the realised net per-capita growth rate (*cf maximum* per-capita growth rate) falls as the population size rises toward the carrying capacity. As the population grows ever closer to its carrying capacity (comes ever-closer to perfect recovery), it grows ever more slowly. Loosely speaking, population recovery can be divided into two phases: a short phase in which population growth is rapid because net per-capita growth is little constrained by population abundance, and a subsequent longer-term phase in which net per-capita growth is low. When the recovery threshold is chosen to be small, the population spends little, or no time in the second (slow-growth) phase before it is deemed to have recovered. Thus, the radius of the downstream plume is jointly determined by the extent of depletion at the edge of the farm (which declines with increasing water velocity) and the water-velocity during the subsequent recovery phase. When the recovery threshold is set large, the population quickly recovers from any 'severe' depletion evident at the farm's downstream edge, but then passes into the slow-growth phase – where it spends most of its recovery time. Thus, the downstream radius of the plume is relatively insensitive to the magnitude of change at the farm-edge, and more directly proportional to the water-velocity.

Turning to the Wilson Bay situation: the long-axis of the farming zone is approximately 5 km. Near surface residual currents in the vicinity of the farm are strongly influenced by wind, but an average value of circa 0.05 m s$^{-1}$ appears probable. We will assume that the residual currents flow along this axis (so giving the maximum possible residence time). Based upon stocking practices, we estimate that mussels may be inducing a mortality of up to 30% d$^{-1}$ amongst those plankton within the dropper-lines (approx. 15% d$^{-1}$ within the farm perimeter once due account is taken of the water below the bottom of the dropper lines). Net mass-specific phytoplankton growth rates

Verification of Firth of Thames hydrodynamic model - Addendum - Interpretation of simulated mussel-farm induced modification of the plankton community relative to the Limits of Acceptable Change criteria: sensitivity of hydrodynamic forcing

75

(in the absence of mussel grazing) can range from (negative; the populations are in decline) through to in excess of 100% d$^{-1}$ (under ideal growing conditions).  At a growth rate of 1 d$^{-1}$, depletion at the downstream edge of the farm is predicted to reach approximately 20% (Figure 1 (a)) when water velocities are low, and to be less than 5% at high water velocities.  Recalling that the Firth-scale LAC states that depletion shall not exceed 20% over more than 10% of the Firth. For a comparison against this threshold it is appropriate to set the recovery-threshold parameter ($\alpha$) to 0.8 (=1-20%/100%) – suggesting that the recovery radius will be no more than approximately 1 km (Figure 1 d.  If $\alpha$ is raised to 0.9, the recovery radius rises to approximately 3 km (Figure 1c).

With this background in mind, let us now discuss the consequences of the flaws that have been revealed in our hydrodynamic simulations.  Since the tidal constituents of the current are well reproduced, we focus upon the residual currents.  We have seen that the speeds of residuals were often (though not invariably) too low, and that, at least at one location, they were often in the wrong direction. We infer that the hydrodynamics used to drive the biological model are such that it may have a tendency to over-predict the magnitude of depletion within the farm and inside the somewhat larger perimeter dictated by the tidal prism around the farm.  Thus, the hydrodynamics are 'worst-case' with respect to the farm-scale LAC criterion (the simulated hydrodynamics are such that a model is more likely to yield results that violate this criterion).  Furthermore, given the manner in which the LAC-criterion is chosen Figure 3(c) suggests that any forecasts based upon under-estimated residual currents may yield over-estimates of the radius of the change-plume.  Thus, the hydrodynamics may also be 'worst-case' with respect to the Firth-scale LAC criterion.

Finally, it is worth noting that Firth-scale LAC makes no stipulation regarding where within the Firth such depletion may (or may not) arise.  Thus, erroneous residual current directions (*cf* speeds) would only matter if they were such that they would cause the simulated plume to be exported from the Firth when, in reality, it would be retained within the Firth.  Inspection of Figures 45-53 within Stephens & Broekhuizen (2003) suggests that false export is not occurring.

**Figure 1.**

(a) Relative size of the surviving population at the downstream perimeter of a hypothetical farm versus the speed of water passage through the farm. (b) to (d) corresponding recovery radii. In (b) the recovery threshold ($\alpha$ of Eq. 4) was set to 0.99, in (c) it was set to 0.90, and in (d) it was 0.8. Other assumptions: farm 5 km long in the axis of water movement; plankton suffer a per-capita mortality of 30% d due to mussels within the farm; carrying capacity was 100 and the maximum specific growth rate was 1 d.
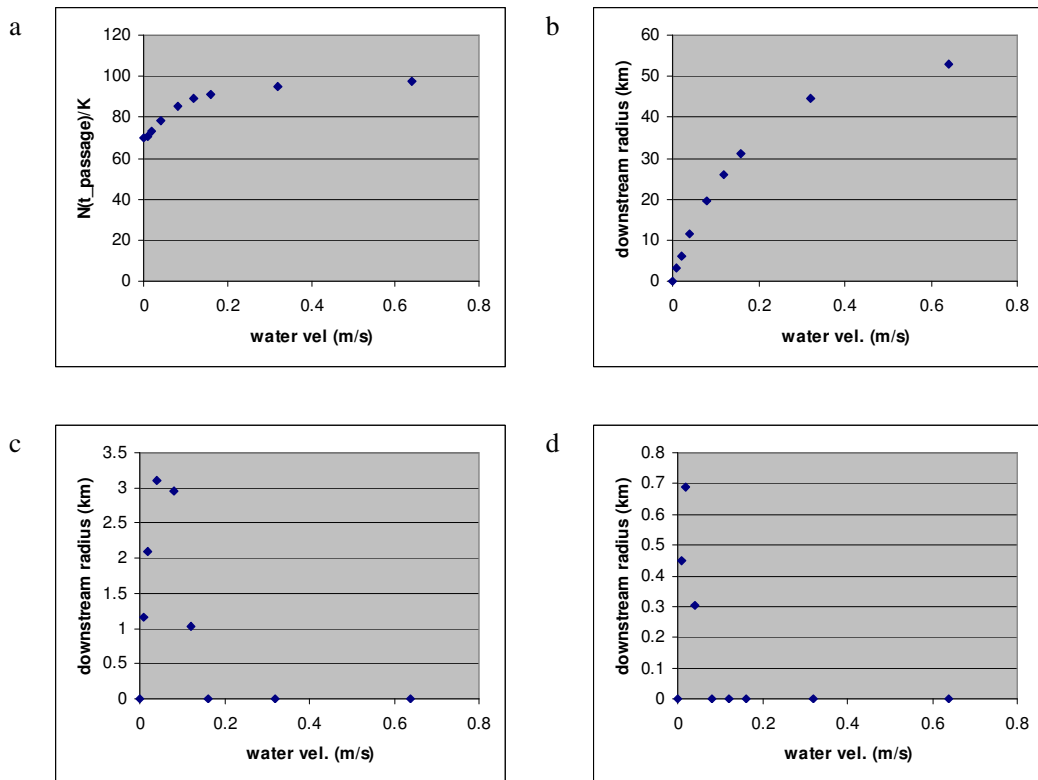
# ₁₃ Numerical simulation

Whilst we believe the above arguments are robust, they rely on some bold simplifying assumptions. It is therefore also appropriate to determine whether the results stemming from a more sophisticated numerical model are sensitive to hydrodynamics when interpreted relative to the two LAC-criteria.

In our original work (Broekhuizen, N.; et al. 2004; Stephens & Broekhuizen 2003), we made simulations for two seasons (early spring and late summer). For each of these, we made simulations under three different wind scenarios. The three wind scenarios resulted in very different residual circulation patterns. Under identical wind-forcing, differing seasonal stratification also induced differences in residual circulation (Stephens & Broekhuizen 2003). These differences are greater than those between observed and simulated residual currents during the two verification periods (i.e., compare the differing residual circulation patterns revealed in Stephens & Broekhuizen (2003) with the magnitudes of discrepancy identified Broekhuizen et al. (2005) and Oldman et al. (2006)). Thus, if we can demonstrate that conclusions drawn by interpreting the results of the biological models relative to the two LAC criteria are insensitive to the (substantial) differences between the hydrodynamic scenarios that we have generated (albeit that these may not be as accurate as we could wish), we have strong evidence that the conclusions would remain similar even if the hydrodynamics were to be improved.

We have repeated some of the Biophysical model (cf logistic model) simulations that Broekhuizen et al. (2004) presented. We used an updated version of the biophysical model. Changes to the biophysical model include: (a) a switch from a Lagrangian to an Eulerian formulation for the plankton, (b) revised description of the attenuation of photosynthetically active radiation based upon recently obtained field data (Broekhuizen & Zeldis 2005), and (c) bug fixes (funding for model development has been through NIWA's Foundation-funded Programs *Sustainable Aquaculture* (contract C01X0507) and *Coasts and Oceans* (contract CO1X0501) and work undertaken for Environment Waikato (Broekhuizen & Zeldis 2005)). This updated version has proven better able to reproduce the patterns of farm-associated plankton change that have been inferred for the Wilson Bay marine farming zone (albeit that it continues to predict an overly strong near-shore/off-shore decline in phytoplankton abundance).

By agreement with Environment Waikato (M. Felsing, V. Pickett, *pers. comm.*, February 7th, 2007), this analysis is restricted to the 'Existing Farms' scenario (i.e., scenario 0 of Broekhuizen et al. (2004); note that in this scenario, Area B of the Wilson's Bay marine farming zone is assumed to be stocked – contrary to the present situation). As previously (Broekhuizen, N.; et al 2004), we have made simulations at two times of the year, and with several different patterns (Table 1).

**Table 1.**

Environmental conditions for which hydrodynamic (and subsequent biological) simulations were made. The season influences factors such as water temperature (hence, stratification) and insolation. Water circulation patters are influenced by factors such as winds and stratification.

| Scenario name | Time of year | Winds |
|---|---|---|
| Sept99 | September | Those of September 1999 |
| ENE Sept | September | Those of 21 Feb – 23 March 1962. Prevailing from ENE |
| WSW Sept | September | Those of 30 June to 30 July 1976. Prevailing from WSW |
| Mar 00 | March | March 2000 |
| ENE Mar | March | Those of 21 Feb – 23 March 1962. Prevailing from ENE |
| WSW Mar | March | Those of 30 June to 30 July 1976. Prevailing from WSW |

Results are presented in Figures 2-7. Of these, Figures 2-4 illustrate the time- and depth-averaged abundance of each of the three phytoplankton taxa under each scenario when farms are absent, and the relative abundance of plankton once the farms are added into the system. Diatoms (Fig. 2) and phytoflagellates (Fig. 3) are predicted to suffer depletion of up to approximately 10% within the Wilson Bay marine farming zone, and the depletion halo extends only 2-3 km beyond the zone's perimeter. Dinoflagellates (Fig. 4) are predicted to suffer higher depletion (up to approximately 20%), and the spatial extent of the depleted zone is much larger. The direction in which the downstream plume of depleted water extends varies amongst the simulations.

The magnitude of within-farm depletion predicted by the numerical model is similar to that forecast by the analytical model. The resolution of the colour-scales in Figures 2-7 is such that depletion of less than approximately 5% cannot be resolved. In the context of the analytical mode, this corresponds to setting $\alpha=0.95$. With that value, the analytical model suggests a recovery radius of 5-6 km (note shown, but see Figure 1 for examples and associated assumptions). This is within a factor of two or so of the radii inferred from the analytical model – which is encouraging given the parameter uncertainties.

Figures 5-7 (respectively, diatoms, phytoflagellates and dinoflagellates) recast the results presented in Figures 2-4 in a manner that facilitates comparison with the two LAC-criteria. The x-axis represents relative biomass (a value of 0.9 indicates that the location- and taxon-specific carbon abundance in the presence of the scenario 0 farms is 90% of that in the absence of those farms, i.e., 10% depletion). The vertical bars indicate what proportion of the Firth's surface area exhibit the corresponding level of relative biomass. The sigmoidal curve is the cumulative density function (CDF) of relative biomass. For any point on the x-axis, the height of the CDF equates to the sum of the histogram bars that lie at that point and to the left of that point (i.e., the value of the curve at a given x-location illustrates what proportion of the Firth exhibits a

Verification of Firth of Thames hydrodynamic model - Addendum - Interpretation of simulated mussel-farm induced modification of the plankton community relative to the Limits of Acceptable Change criteria: sensitivity of hydrodynamic forcing

79

relative biomass that is less than, or equal to the relative biomass). The intersection-point of the vertical and horizontal dotted lines corresponds to the Firth-scale LAC-criterion. The intersection-point of the vertical and horizontal dashed lines corresponds to the Farm-scale LAC-criterion. Note that the LAC-criteria are formulated in terms of relative change in chlorophyll abundance (an easily measured indicator of total phytoplankton abundance). The model measures taxon-specific phytoplankton abundance in terms of carbon. If taxon-specific carbon: chlorophyll ratios were constant, the differing units would be irrelevant. In reality carbon:chlorophyll ratios can vary (circa two-fold within a taxon) in response to environmental conditions. If environmental conditions are such that carbon:chlorophyll ratios vary in space (*cf* time), the implication is that depletion patterns measured in terms of carbon may differ a little from those measured in terms of chlorophyll.

If it is accepted that carbon and chlorophyll are highly correlated, then so long as the intersection of the solid (sigmoidal) curve and the horizontal dotted line is to the right of the vertical dotted line, the Firth-scale 20%/10% criterion is not being violated for the taxon in question. Similarly, if the solid curve intersects the horizontal dashed line to the right of the vertical dashed line, the farm-scale LAC-criterion is not being violated. The LAC is posed in terms of total chlorophyll (rather than taxon-specific biomass), but the former is merely a weighted average of the component taxon-specific abundances. Clearly the sigmoidal curve intersects with the horizontal lines well to the right of the corresponding vertical lines – even for dinoflagellates (which are the most seriously depleted). Furthermore, within each taxon, the shapes and locations (along the x-axis) of the CDF are very similar in all six wind/season scenarios. For example, across the six wind/season scenarios, the maximum depletion time-averaged dinoflagellate depletion measured in any of water-columns varied only around two-fold: between approximately 12% (September WSW scenario) and 24% (March ENE scenario). The fraction of the Firth suffering 20% or more depletion (i.e., the depletion threshold that would throw the Firth-scale LAC-criterion if it were exceeded over more than 10% of the Firth) was less than about 2% (e.g., March WSW scenario).

**Figure 2.**

Left-hand panel of each pair: simulated time-average carbon abundance (left-hand panel, log₁₀(mg C m-3) of <u>diatoms</u> in the upper 20 m of the water-column (in the absence of farms). Right hand-column of each pair: relative time-averaged biomass in the presence of farms. Values below 1.0 imply depletion. The time-average was from day 10 of the simulation until the end of the simulation.

Verification of Firth of Thames hydrodynamic model - Addendum - Interpretation of simulated mussel-farm induced modification of the plankton community relative to the Limits of Acceptable Change criteria: sensitivity of hydrodynamic forcing

81
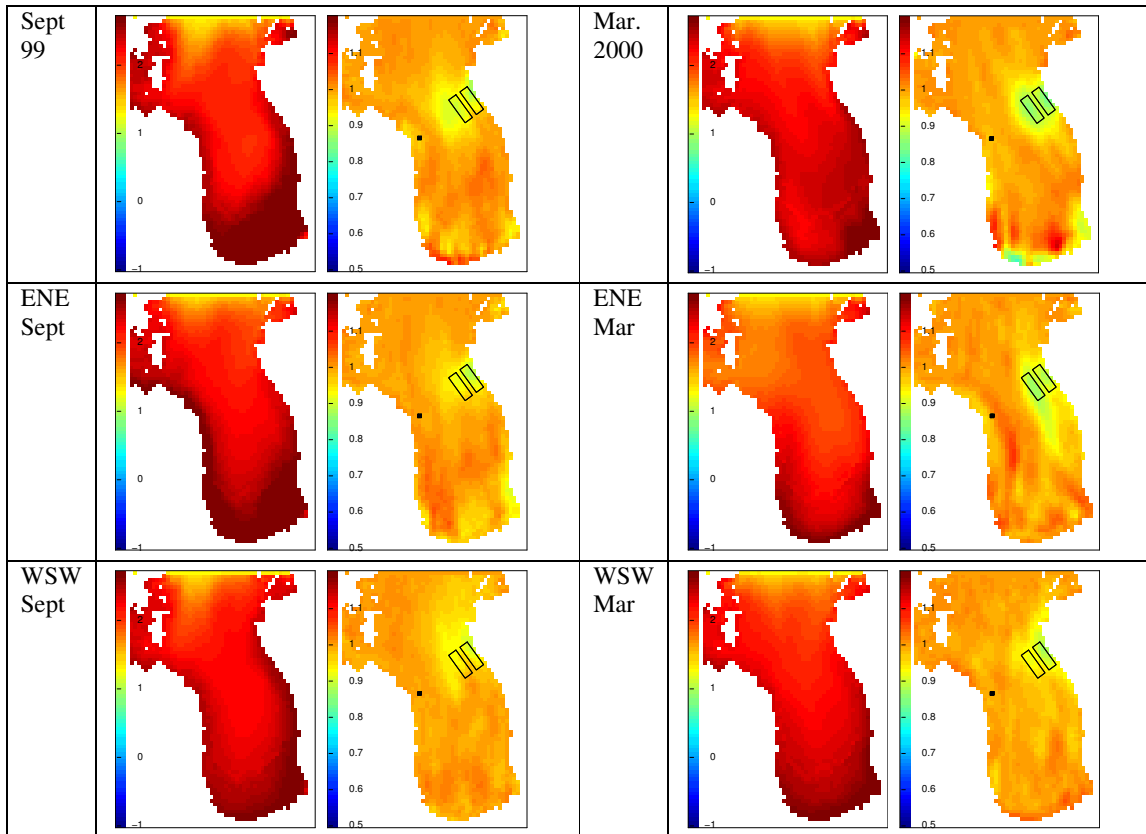
**Figure 3.**

Left-hand panel of each pair: simulated time-average carbon abundance (left-hand panel, $\log_{10}$ (mg C m$^{-3}$) of <u>phytoflagellates</u> in the upper 20 m of the water-column (in the absence of farms). Right hand-column of each pair: relative time-averaged biomass in the presence of farms. Values below 1.0 imply depletion. The time-average was from day 10 of the simulation until the end of the simulation.

Verification of Firth of Thames hydrodynamic model - Addendum - Interpretation of simulated mussel-farm induced modification of the plankton community relative to the Limits of Acceptable Change criteria: sensitivity of hydrodynamic forcing

82
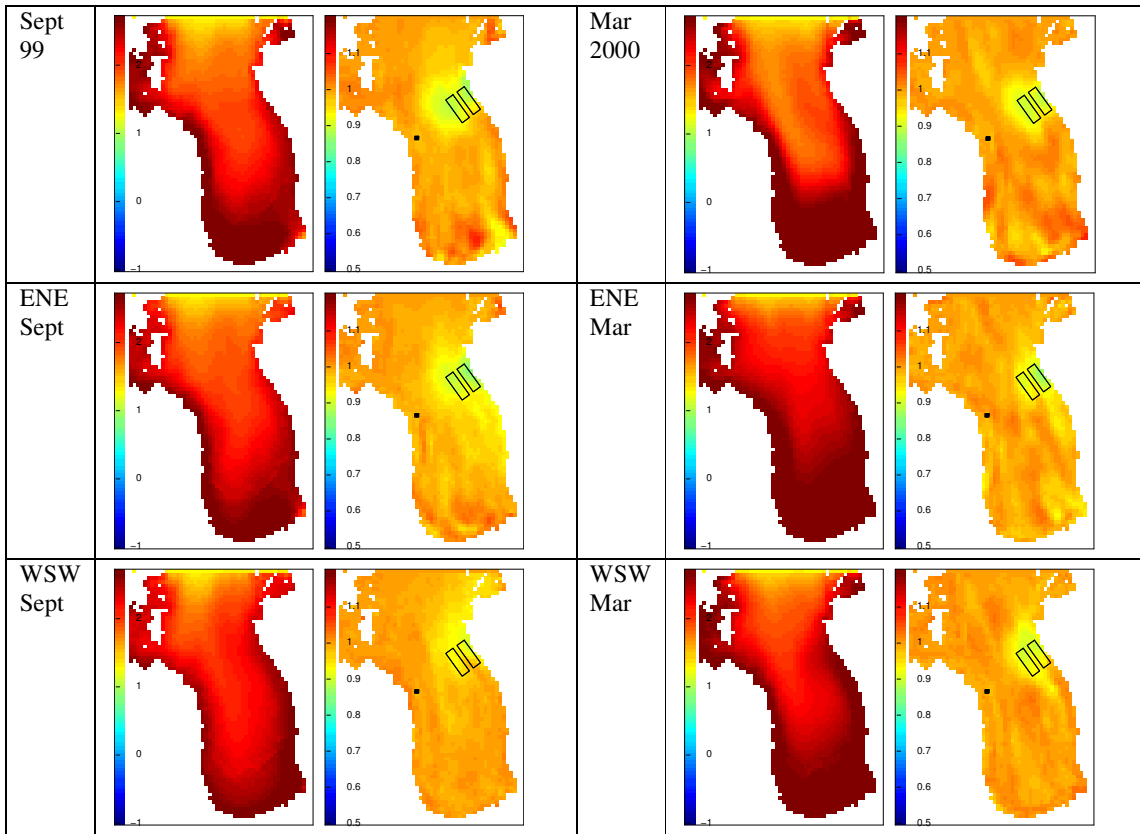
**Figure 4.**

Left-hand panel of each pair: simulated time-average carbon abundance (left-hand panel, $\log_{10}$ (mg C m$^{-}$) of <u>dinoflagellates</u> in the upper 20 m of the water-column (in the absence of farms). Right hand-column of each pair: relative time-averaged biomass in the presence of farms. Values below 1.0 imply depletion. The time-average was from day 10 of the simulation until the end of the simulation.

Verification of Firth of Thames hydrodynamic model - Addendum - Interpretation of simulated mussel-farm induced modification of the plankton community relative to the Limits of Acceptable Change criteria: sensitivity of hydrodynamic forcing

83
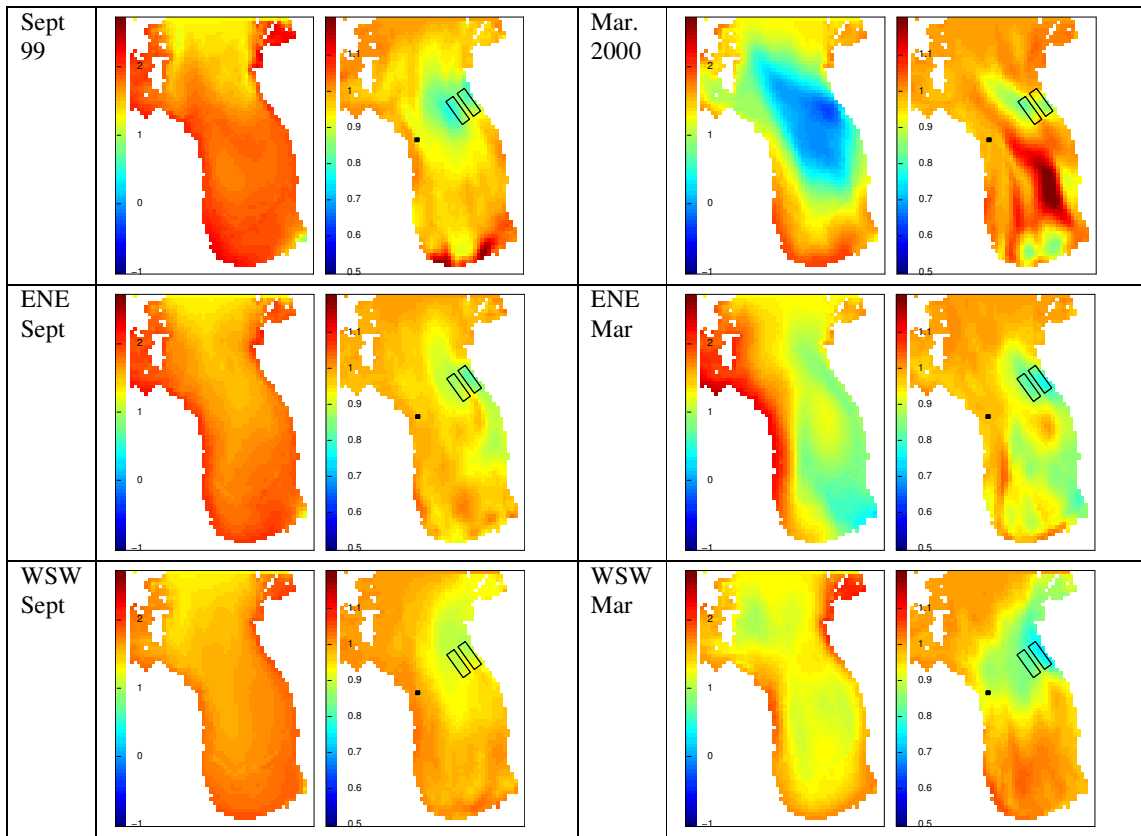
**Figure 5.**

Probability (histogram) and cumulative probability distributions (solid curve) for relative change in
time averaged diatom abundance in the presence of mussel farms at Waimangu Point and
Wilsons Bay Areas A & B in each wind/season hydrodynamic scenario. The intersection of the
dotted lines is the Firth-scale LAC-criterion for plankton depletion. The intersection of the dashed
lines is the farm-scale LAC-criterion.
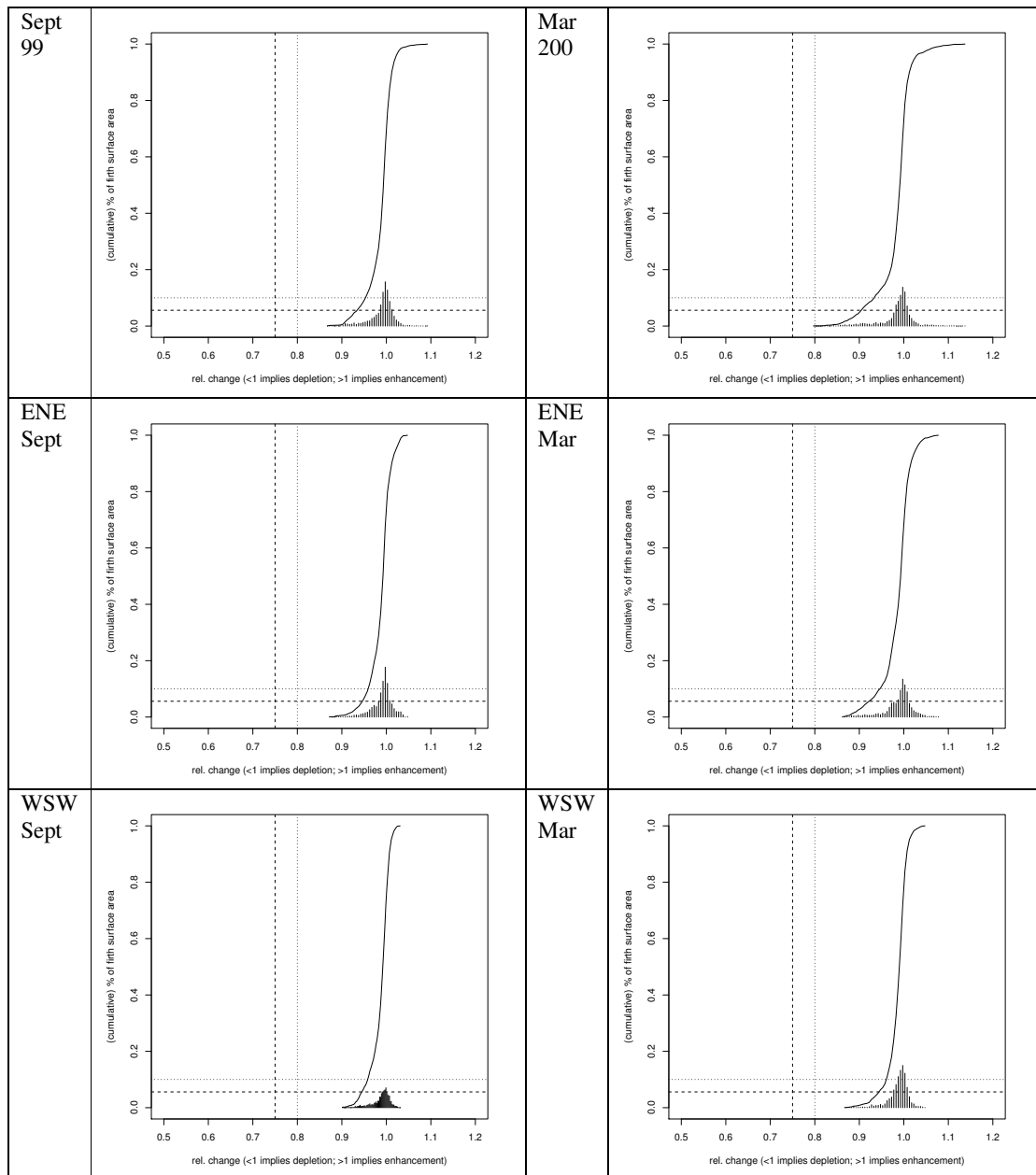
**Figure 6.**

Probability (histogram) and cumulative probability distributions (solid curve) for relative change in time averaged phytoflagellate abundance in the presence of mussel farms at Waimangu Point and Wilsons Bay Areas A & B in each wind/season hydrodynamic scenario. The intersection of the dotted lines is the Firth-scale LAC-criterion for plankton depletion. The intersection of the dashed lines is the farm-scale LAC-criterion.
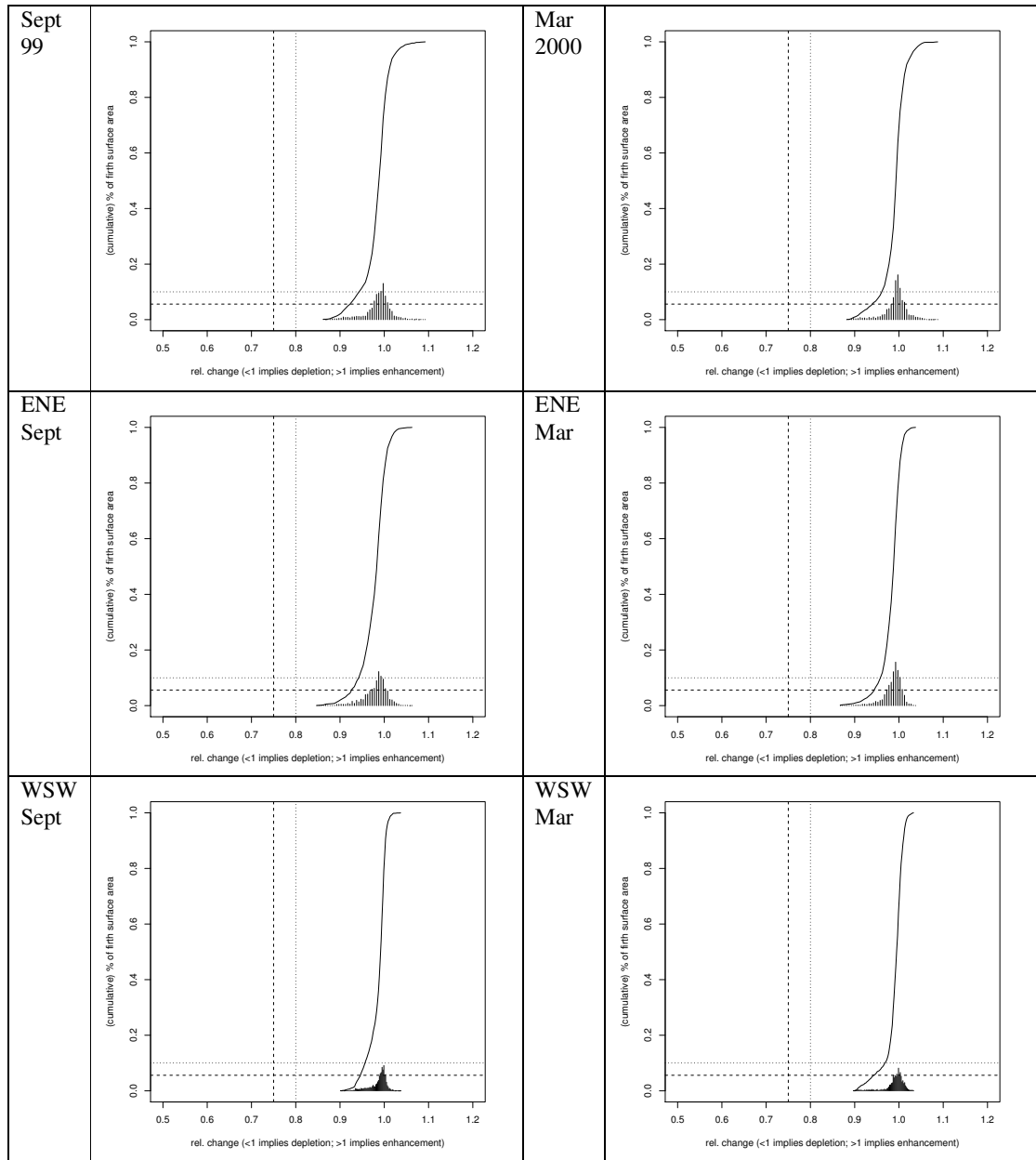
**Figure 7.**

Probability (histogram) and cumulative probability distributions (solid curve) for relative change in time averaged dinoflagellate abundance in the presence of mussel farms at Waimangu Point and Wilsons Bay Areas A & B in each wind/season hydrodynamic scenario. The intersection of the dotted lines is the Firth-scale LAC-criterion for plankton depletion. The intersection of the dashed lines is the farm-scale LAC-criterion. Provided that the solid curve intersects with each horizontal line to the right of the intersection of the horizontal line and the corresponding vertical line, the criteria are not being broken.
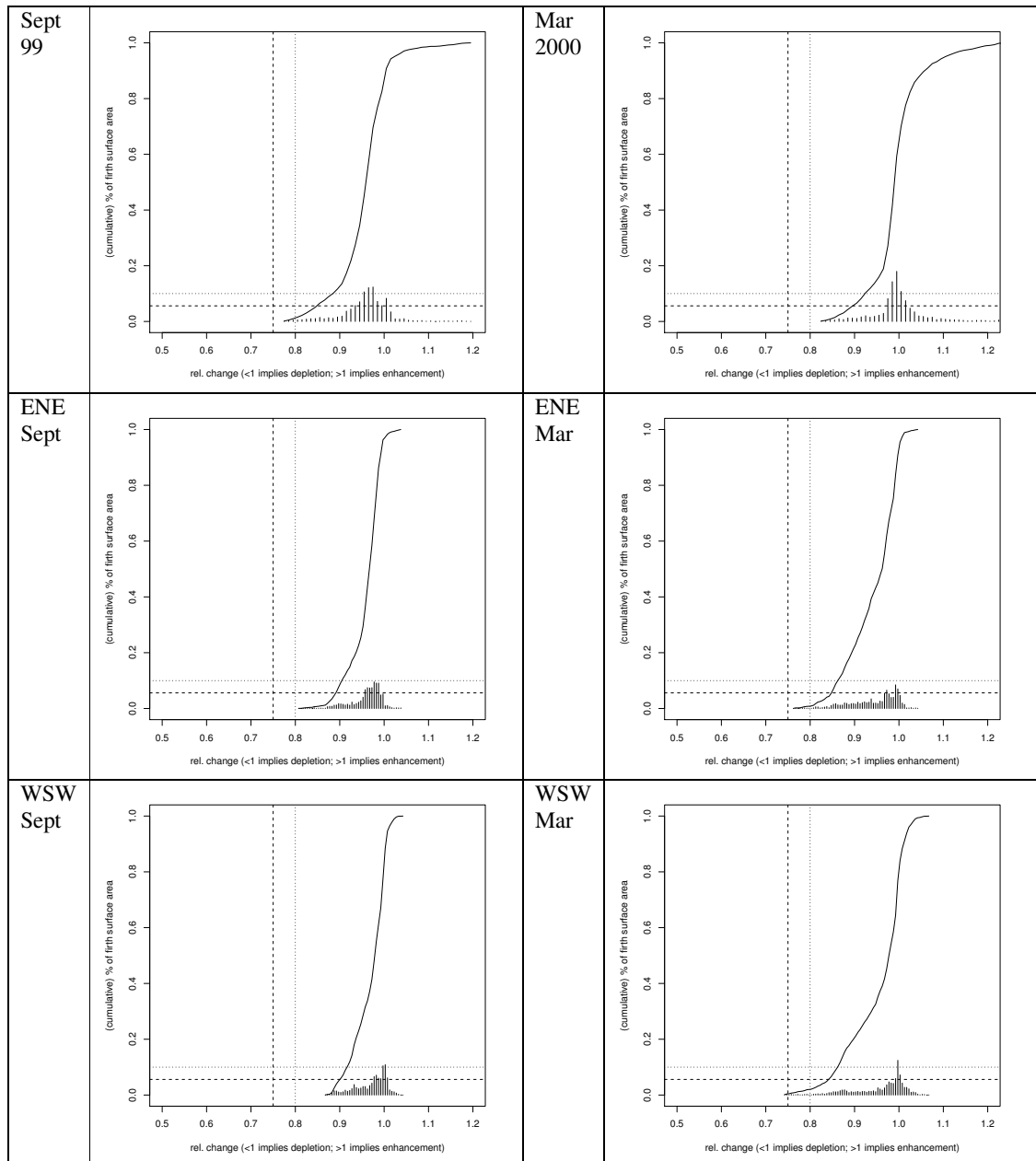
# 14 Conclusions

In the context of a discussion about <u>sensitivity to inaccurate residual currents and stratification</u>, the key conclusion from the simulations presented above is that, under all the season/wind scenarios the biophysical model indicates levels of plankton depletion that are far-separated from the LAC-threshold values. The differences between the residual currents associated with each of the six scenarios are much greater than those between observed and simulated residual currents (and stratification) in each of the two verification periods. Thus, we conclude that <u>with respect to the LAC-criteria (and at the stocking levels envisaged in these simulations)</u>, results stemming from the biophysical model are insensitive to hydrodynamic errors of the magnitudes that have been identified.

It is important to realise that it is only with respect to the LAC-criteria that the results from the biological model are insensitive to the hydrodynamics. The location of the plume of plankton change is strongly influenced by the residual currents – this is especially evident for the dinoflagellates. It is clear that the performance of the hydrodynamic model will need to be improved before it (or models dependent upon it) can be applied to questions concerning location-specific downstream effects.